Volume 6, Issue 11 – July – December – 2020

ECORFAN

Journal-Democratic Republic of Congo

ISSN-On line 2414-4924

ECORFAN®

ECORFAN Journal - Democratic Republic of Congo, Volume 6, Issue 11, July-December 2020, is a journal edited semestral by ECORFAN. 6593 Kinshasa 31 Rép.DémocratiqueduCongo.WEB:www.ecorfan.org/DemocraticRepublicofCongo/, journal@ecorfan.org. Editor in Chief: ILUNGA-MBUYAMBA, Elisée. MsC. ISSN On line: 2414-4924. Responsible for the latest update of this number ECORFAN Computer Unit. ESCAMILLA-BOUCHÁN, Imelda. PhD, LUNA-SOTO, Vladimir. PhD, 6593 Kinshasa 31 Rép. Démocratique du Congo, last updated December 31, 2020.

ECORFAN-Democratic Republic of Congo

Definition of Journal

Scientific Objectives

Support the international scientific community in its written production Science, Technology and Innovation in the Field of Physical Sciences Mathematics and Earth sciences, in Subdisciplines of image and signal processing, control-digital system-artificial, intelligence-fuzzy, logic-mathematical, modeling-computational, mathematics-computer, science.

ECORFAN-Mexico SC is a Scientific and Technological Company in contribution to the Human Resource training focused on the continuity in the critical analysis of International Research and is attached to CONACYT-RENIECYT number 1702902, its commitment is to disseminate research and contributions of the International Scientific Community, academic institutions, agencies and entities of the public and private sectors and contribute to the linking of researchers who carry out scientific activities, technological developments and training of specialized human resources with governments, companies and social organizations.

Encourage the interlocution of the International Scientific Community with other Study Centers in Mexico and abroad and promote a wide incorporation of academics, specialists and researchers to the publication in Science Structures of Autonomous Universities - State Public Universities - Federal IES - Polytechnic Universities - Technological Universities - Federal Technological Institutes - Normal Schools - Decentralized Technological Institutes - Intercultural Universities - S & T Councils - CONACYT Research Centers.

Scope, Coverage and Audience

ECORFAN-Democratic Republic of Congo is a Journal edited by ECORFAN-Mexico S.C in its Holding with repository in Democratic Republic of Congo, is a scientific publication arbitrated and indexed with semester periods. It supports a wide range of contents that are evaluated by academic peers by the Double-Blind method, around subjects related to the theory and practice of image and signal processing, control-digital system-artificial, intelligence-fuzzy, logic-mathematical, modeling-computational, mathematics-computer, science with diverse approaches and perspectives , That contribute to the diffusion of the development of Science Technology and Innovation that allow the arguments related to the decision making and influence in the formulation of international policies in the Field of Physical Sciences Mathematics and Earth sciences. The editorial horizon of ECORFAN-Mexico® extends beyond the academy and integrates other segments of research and analysis outside the scope, as long as they meet the requirements of rigorous argumentative and scientific, as well as addressing issues of general and current interest of the International Scientific Society.

Editorial Board

Arbitration Committee

Assignment of Rights

The sending of an Article to ECORFAN-Democratic Republic of Congo emanates the commitment of the author not to submit it simultaneously to the consideration of other series publications for it must complement the Originality Format for its Article.

The authors sign the Authorization Format for their Article to be disseminated by means that ECORFAN-Mexico, S.C. In its Holding Democratic Republic of Congo considers pertinent for disclosure and diffusion of its Article its Rights of Work.

Declaration of Authorship

Indicate the Name of Author and Coauthors at most in the participation of the Article and indicate in extensive the Institutional Affiliation indicating the Department.

Identify the Name of Author and Coauthors at most with the CVU Scholarship Number-PNPC or SNI-CONACYT- Indicating the Researcher Level and their Google Scholar Profile to verify their Citation Level and H index.

Identify the Name of Author and Coauthors at most in the Science and Technology Profiles widely accepted by the International Scientific Community ORC ID - Researcher ID Thomson - arXiv Author ID - PubMed Author ID - Open ID respectively.

Indicate the contact for correspondence to the Author (Mail and Telephone) and indicate the Researcher who contributes as the first Author of the Article.

Plagiarism Detection

All Articles will be tested by plagiarism software PLAGSCAN if a plagiarism level is detected Positive will not be sent to arbitration and will be rescinded of the reception of the Article notifying the Authors responsible, claiming that academic plagiarism is criminalized in the Penal Code.

Arbitration Process

All Articles will be evaluated by academic peers by the Double Blind method, the Arbitration Approval is a requirement for the Editorial Board to make a final decision that will be final in all cases. MARVID® is a derivative brand of ECORFAN® specialized in providing the expert evaluators all of them with Doctorate degree and distinction of International Researchers in the respective Councils of Science and Technology the counterpart of CONACYT for the chapters of America-Europe-Asia-Africa and Oceania. The identification of the authorship should only appear on a first removable page, in order to ensure that the Arbitration process is anonymous and covers the following stages: Identification of the Journal with its author occupation rate - Identification of Authors and Coauthors - Detection of plagiarism PLAGSCAN - Review of Formats of Authorization and Originality-Allocation to the Editorial Board- Allocation of the pair of Expert Arbitrators-Notification of Arbitration - Declaration of observations to the Author-Verification of Article Modified for Editing-Publication.

Instructions for Scientific, Technological and Innovation Publication

Knowledge Area

The works must be unpublished and refer to topics of Image and signal processing, control-digital system-artificial, intelligence-fuzzy, logic-mathematical, modeling-computational, mathematics-computer, science and other topics related to Physical Sciences Mathematics and Earth sciences.

Presentation of the Content

In the first article we present, *Methodology to calculate the density of the magnetic field generated in overhead transmission lines in HVDC applying a two-dimensional analysis of parallel poles above ground level*, by AGUILAR-MARIN, Jorge Luis, CISNEROS-VILLALOBOS, Luis, PADILLA-CANTERO, Jorge Gabriel and VERGARA-VÁZQUEZ, Julio Cesar, with adscription in the Universidad Autónoma del Estado de Morelos, as the next article we present, *A brief description of the GPS architecture*, by MEDINA-CASTRO, Paul, CARAVEO-MENA, Camilo, BARBOZA-TELLO, Norma Alicia and LOREDO-MEDINA, Raúl, with adscription in the Universidad Autónoma de Baja California and Instituto Tecnológico Superior de Guasave, as the next article we present, *Heuristic study of a full can implementation on a network of digital controllers based on experimental data*, by LUJÁN-RAMÍREZ, Carlos Alberto, SANDOVAL-GÍO, Jesús, FLORES-NOVELO, Agustín Alfonso and OJEDA-ARANA, Juan Alberto, with adscription in Tecnológico Nacional De México / I.T. Mérida, as the last article we present, *Hydrodynamic analysis of different impellers used in the stir casting process*, by PÉREZ-PÉREZ, Arnulfo, MARTÍNEZ-VÁZQUEZ, J. Merced, RODRÍGUEZ-ORTIZ, Gabriel and GARCÍA-DUARTE, Oscar Enrique, with adscription in the Universidad Politécnica de Juventino Rosas.

Content

Article ECORFAN Journal Democratic Republic of Congo
December 2020 Vol.6 No.11 1-11

Methodology to calculate the density of the magnetic field generated in overhead transmission lines in HVDC applying a two-dimensional analysis of parallel poles above ground level

Metodología para calcular la densidad del campo magnético generado en líneas de transmisión aéreas en HVDC aplicando un análisis bidimensional de polos paralelos sobre el nivel del suelo

AGUILAR-MARIN, Jorge Luis†*, CISNEROS-VILLALOBOS, Luis, PADILLA-CANTERO, Jorge Gabriel and VERGARA-VÁZQUEZ, Julio Cesar

Universidad Autónoma del Estado de Morelos, Faculty the Chemical Sciences and Engineering, Av. University 1001, Cuernavaca, Morelos, C.P. 62209, Mexico.

ID 1st Author: *Jorge Luis, Aguilar-Marin* / **ORC ID:** 0000-0002-0235-6946, **Researcher ID:** ABD-4533-2020, **CVU CONACYT ID:** 1010823

ID 1st Co-author: *Luis, Cisneros-Villalobos* / **ORC ID:** 0000-0002-9409-1374, **Researcher ID:** ABD-4724-2020, **CVU CONACYT ID:** 82259

ID 2nd Co-author: *Jorge Gabriel, Padilla-Cantero* / **ORC ID:** 0000-0002-6414-9483, **Researcher ID:** ABD-5334-2020

ID 3rd Co-author: *Julio Cesar, Vergara-Vázquez* / **ORC ID:** 0000-0003-1524-7914, **Researcher ID:** ABD-5487-2020

DOI: 10.35429/EJDRC.2020.6.11.1.11 Received July 10, 2020; Accepted December 30, 2020

Abstract

The growth in the demand for electricity has led to the development and application of technologies that make its means of transport more efficient. Thus, one of these options is the implementation of transmission lines in HVDC. One of important design parameters of these lines is to know their magnetic field distribution, when it is required to calculate it, there is no methodology that can be applied to HVDC transmission lines. The following article presents a methodology that allows obtaining the density of the magnetic field on the corridor of an overhead transmission line. A case study of a 500 kV bipolar line in HVDC is presented, the results obtained are compared using the commercial software Field and corona Effects (FACE), the results obtained are consistent with those obtained from the presented methodology. An analysis of the impact of the transmission line configuration on the magnetic field density is developed, defining the most efficient configuration.

HVDC, Imaginary poles, Line runner

Resumen

El crecimiento de la demanda de energía eléctrica ha provocado el desarrollo y la aplicación de tecnologías que hacen más eficiente su medio de transporte. Así una de estas operaciones es la implementación de líneas de transmisión en HVDC. Uno de los parámetros importantes de diseño de estas líneas es conocer su distribución de su campo magnético, cuando se requiere calcularlo no se cuenta con una metodología que pueda ser aplicada en las líneas de transmisión en HVDC. El siguiente artículo presenta una metodología que permite la obtención de la densidad del campo magnético sobre el corredor de una línea de transmisión aérea. Se presenta un caso de estudio de una línea bipolar de 500 kV en HVDC, los resultados obtenidos son comparados por medio del software comercial Field and Corona Effects (FACE), los resultados obtenidos son coherentes con los obtenidos a partir de la metodología presentada. Se desarrolla un análisis del impacto de la configuración de la línea de transmisión en la densidad de campo magnético, definiendo la configuración más eficiente.

HVDC, Polos imaginarios, Corredor de línea

Citation: AGUILAR-MARIN, Jorge Luis, CISNEROS-VILLALOBOS, Luis, PADILLA-CANTERO, Jorge Gabriel and VERGARA-VÁZQUEZ, Julio Cesar. Methodology to calculate the density of the magnetic field generated in overhead transmission lines in HVDC applying a two-dimensional analysis of parallel poles above ground level. Journal - Democratic Republic of Congo. 2020. 6-11:1-11.

* Correspondence to Author (Email: jorge.aguilar.itt@gmail.com)
† Researcher contributing as first author.

Article ECORFAN Journal Democratic Republic of Congo
December 2020 Vol.6 No.11 1-11

Introduction

Today, one of the most efficient methods for the transmission of electrical energy is to use High Voltage Direct Current (HVDC), when it comes to providing electrical energy from long distances to a large load and that is in continuous growth (Lee, Pong & Zhu, 2019), (Tang, Luo & Wei, 2013), (Feltes, Gemmell & Retzmann, 2011).

Due to the remarkable increase in the power and reliability of AC/DC power converters, the transmission of high voltage power in HVDC has grown significantly worldwide. Currently, the voltages used for overhead transmission are in the range of ±500 to ±800 kV, with nominal currents of 1 to 4 kA (Girdinio, Molfino, Nervi, Rossi, Bertani & Malgarotti, 2015), (Baharman & Johnson, 2007).

The below the main ones are listed technical benefits of an HVDC system (Samy, 2017).

– The energy flow is fully controllable, fast and accurate.

– The link in HVDC is asynchronous and can adapt to any nominal voltage or frequency.

– Transmission lines in HVDC do not increase the short-circuit level of the system and faults cannot be transferred through connections in HVDC.

– There is a better ability to transmit power with overhead, underground and submarine cables over long distances.

– The visual impact and the use of the land is lower, as well as the cost for the line corridor (Mooney, 2010).

In Figure 1 the dimensions of the land used for transmission line are observed HVAC and an HVDC (Zhou, Qiu, Sun, Chen, Deng, Qian, Wang, Zhao, Li, Li, Qiu & Yu, 2018).

Currently Mexico does not have transmission systems in HVDC and with the growing demand for energy, it will be one of the most efficient transmission media in the near future, so this technology is being analysed by Mexican regulations, for the development of the National Electric System (SEN), with regard to generation and transmission activities (PROSEDEN, 2019).

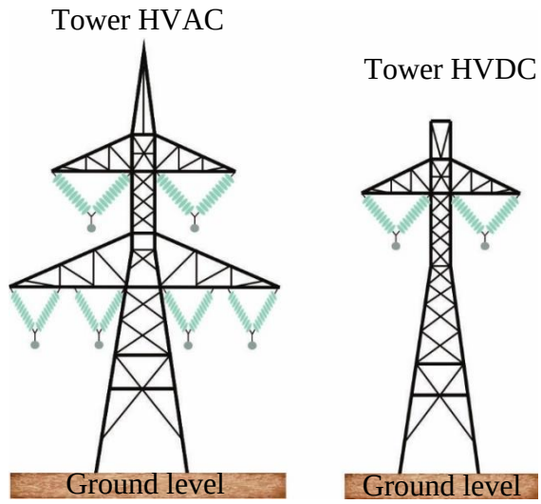

Figure 1 High voltage structures in HVAC and HVDC
Source: Own elaboration

One of the important parameters for the design of HVDC lines is the magnetic field is caused by the circulation of electric current in a conductor (Jang, Kim, Lee, Lim & Sood, 2009), (Rofalski & Schlabbach, 2014). Figure 2 shows its distribution around a conductor, so the magnetic field generated in transmission lines is determined by the magnitude of the current that circulates through the conductors and by the spatial configuration of the line (IEC, 2014).

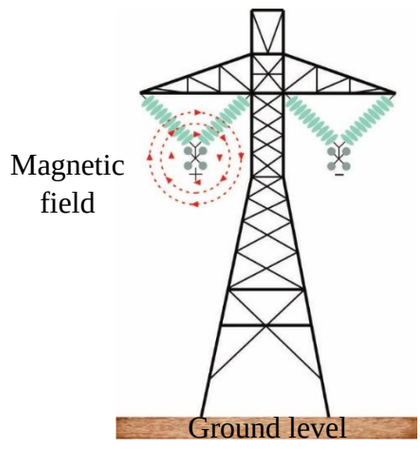

Figure 2 Magnetic field in a bipolar transmission line in HVDC
Source: Own elaboration

ISSN: 2414-4924

AGUILAR-MARIN, Jorge Luis, CISNEROS-VILLALOBOS, Luis, PADILLA-CANTERO, Jorge Gabriel and VERGARA-VÁZQUEZ, Julio Cesar. Methodology to calculate the density of the magnetic field generated in overhead transmission lines in HVDC applying a two-dimensional analysis of parallel poles above ground level. Journal - Democratic Republic of Congo. 2020

In the case of HVDC systems the frequency is null, therefore is it considered 0 Hz, according to the Carson method (Zhu, Lee & Pong, 2018). The image conductor will be located at a great depth below ground level as seen in Figure 3 and the equivalent distance of the image conductor will tend to infinity (IEC, 2014) therefore, the effect of the image conductors is so small that can despised for the calculation of the magnetic field density in HVDC transmission lines.

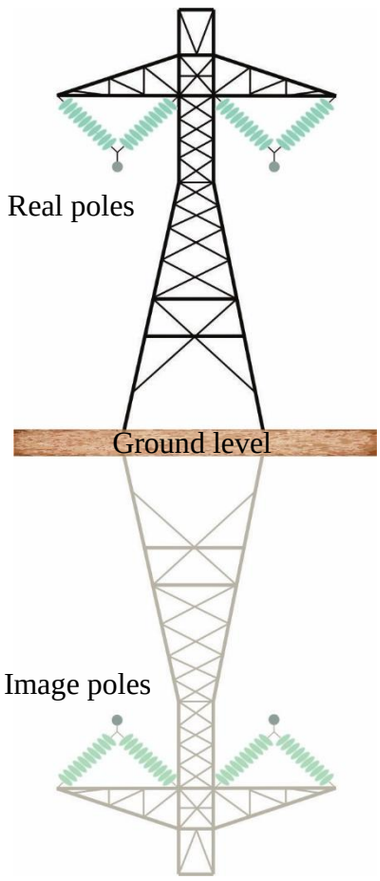

Figure 3 Carson´s method, imaginary poles.
Source: Own elaboration

At present there are multiple software is that present the calculation of the magnetic field density of HVDC transmission lines such as CRmag, FACE, ETAP, among others. However, most require the purchase of licenses for their operation.

This software's are based, on the method complex penetration, which uses Carson´s method that consists of the circulation of a current that returns overland, this method considers the ground as a superconductor, based on the phenomenon of the skin effect or complex penetration effect, with which the return of the current through the ground is modelled.

The complex penetration effect considers that the magnetic field lines cross the surface of the soil, where for the calculation magnetic field density the equivalent complex reference plane is considered, which is at a great depth, to know this depth. The parameter α related to the skin depth or complex penetration depth, or the distance from the ground level surface to the reference plane is incorporated (Sarma, 2000).

The following article provides engineers with a reference methodology, which contains the steps necessary to calculate the magnetic field density for the first overhead transmission lines in HVDC to be built in Mexico. The density of the magnetic field is obtained by applying a two-dimensional analysis of the transmission line, assuming parallel poles above ground level, considering the operating characteristics of the line and, unlike other methodologies, the exposure limits to magnetic fields are taken into account recommended by (ICNIRP, 2009). The methodology offers speed and precision in calculating the density of the magnetic field over the corridor of a monopolar and bipolar transmission line.

Calculation methodology for density of magnetic field

The following methodology allows calculate the components of the magnetic field density in a simplified but reasonably exact way over the corridor of an overhead transmission line in HVDC, the design is based mainly on complying with the limits for exposure to magnetic fields. The flow chart of the methodology is presents itself ted in Figure 4.

ISSN: 2414-4924

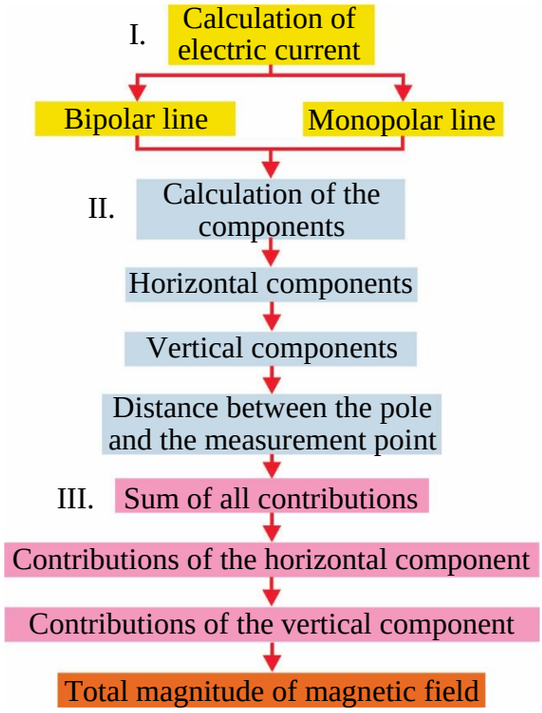

Figure 4 Process for calculating the magnetic field density in HVDC transmission lines
Source: Own elaboration

Calculation of the electric current

The calculation of electric current intensity for transmission lines in monopolar and bipolar HVDC It is determined through the equations (1) and (2), respectively (CIGRE, 2014).

$$I = \frac{1}{2} \cdot \left(\frac{P \times 10^3}{V}\right) A \quad (1)$$

$$I = \left(\frac{P \times 10^3}{V}\right) A \quad (2)$$

Where:

I = Electric Current of the pole, in A.
P = Power of the line, in MW.
V = Electrical voltage of the pole, in kV.

The current intensity will considered positive, when evaluating the positive pole and negative when considering the negative pole (CIGRE, 2014).

Calculation of horizontal and vertical components

To determine the components of the magnetic field density, the following considerations must taken.

- The currents at the poles of transmission lines in HVDC are of different polarity, which reduces the magnetic field density. For a monopolar transmission line, the magnetic field density is higher (CIGRE, 2014).
- The currents at the poles they only contribute with its real component (CIGRE, 2014).

Using the previous considerations, the contributions of the magnetic field density due to the effect of the current in each of the components (horizontal and vertical) are obtained.

Figure 5 shows the horizontal and vertical components of the magnetic field at a point P, on the axis of the coordinates (x, y) located at a height of 1 m above the transmission line corridor (CIGRE, 2014), (IEEE, 2002).

The horizontal and vertical components are obtained by applying equations (3) and (4) respectively (CIGRE, 2014).

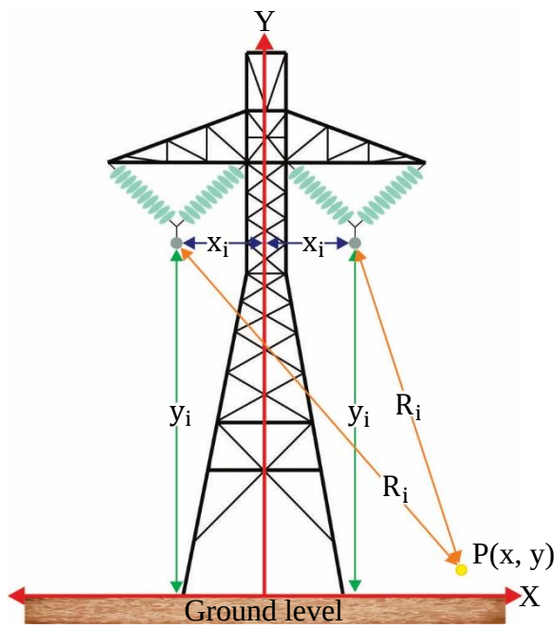

Figure 5 Horizontal and vertical components.
Source: Own elaboration

For the horizontal components, equation (3) is used.

$$B_{x_i} = \frac{\mu_0 \cdot I}{2 \times 10^{-6} \cdot \pi} \cdot \left(\frac{x - x_i}{R_i^2}\right) \mu T \quad (3)$$

For the vertical components, equation (4) is used.

$$B_{y_i} = \frac{\mu_0 \cdot I}{2\times10^{-6}\cdot\pi} \cdot \left(\frac{y-y_i}{R_i^{\,2}}\right) \mu T \quad (4)$$

Where:

B_{x_i} = Horizontal component of the pole magnetic field, in μT.
B_{y_i} = Vertical component of pole magnetic field, in μT.
μ_0 = Magnetic permeability of vacuum $4 \cdot \pi x10^{-7}$, in $\frac{H}{m}$.
X = Coordinate on the horizontal axis of the measurement point P, in m.
Y = Coordinate on the vertical axis of the measurement point P, in m.
x_i = Coordinate on the horizontal axis of the pole, in m.
y_i = Coordinate on the vertical axis of the pole, in m.
R_i = Distance between pole and measuring point P, in m.

The distance between the pole and the measurement point P, is obtained with equation (5).

$$R_i = \sqrt{(x-x_i)^2 + (y-y_i)^2}\ m \quad (5)$$

Sum of all contributions at a point

The magnetic field at the measurement point P, under the transmission line, will be the sum of the contributions from the poles and are obtained by applying equations (6) and (7) (CIGRE, 2014).

$$B_H = \sum_{i=1}^{u} B_{x_i}\ \mu T \quad (6)$$

$$B_V = \sum_{i=1}^{u} B_{y_i}\ \mu T \quad (7)$$

Where:

B_H = Horizontal component of magnetic field under the line at measurement point P, in μT.
B_V = Vertical component of magnetic field under the line at the measurement point P, in μT.
u = Number of poles present in the line.

The total magnetic field at the measurement point P is obtained by applying equation (8).

$$B_T = \sqrt{B_H^{\,2} + B_V^{\,2}}\ \mu T \quad (8)$$

Where:

B_T = Total magnitude of magnetic field at measurement P, in μT.

The International Commission on Non-Ionizing Radiation Protection (ICNIR) and the International Radiological Protection Association (IRPA) recommend that the limit of public exposure to magnetic field in transmission lines in HVDC should be less than 40 mT (ICNIRP, 2009).

Case study

Consider a 500 kV bipolar transmission line in HVDC where you want to calculate the density of the magnetic field at one meter above ground level, over a 120 m corridor of line. Table 1 shows the spatial measurements of the pole locations of the bipolar line. Figure 6 shows the configuration of the transmission tower, the spacing between the posts and its location above ground level. Table 2 shows the operating characteristics of the line.

Conductor	x axis	y axis
Positive pole	-10 m	20 m
Negative pole	10 m	20 m

Table 1 Coordinates of the poles in the bipolar transmission line
Source: Own elaboration

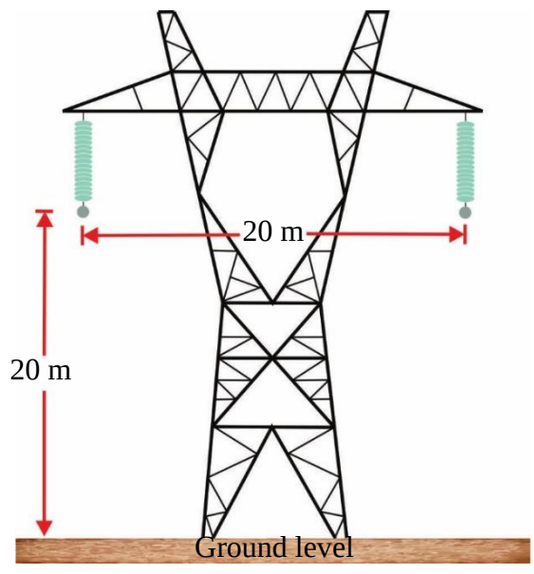

Figure 6 Profile of the 500 kV bipolar transmission line in HVDC
Source: (Lee, Pong & Zhu, 2019)

Operation characteristics	Value per unit
Tension electrical rating	500 kV
Electrical rated power	3000 MW
Type of conductor	ACSR 1590
Separation between poles	20 m
Height of the poles	20 m

Table 2 Specifications of the bipolar transmission line
Source: Own elaboration

Calculation of the electric current

The electric current is obtained using equation (1).

$$I = \frac{1}{2} \cdot \left(\frac{3000 \times 10^3}{500} \right) = 3000 \text{ A}$$

Calculation of horizontal and vertical components

The distance from the pole to the measurement point P is obtained by equation (5), IEEE recommends that the magnetic fields density calculation be considered at a height of 1 m above ground level along the transmission line corridor (IEEE, 1994), using intervals of 10 m from the line corridor.

Considering a point P (x = 0, y = 1), for the positive pole.

$$R_1 = \sqrt{(0 - (-10))^2 + (1 - 20)^2}$$
$$R_1 = 21.4709 \text{ m}$$

For the rest of the intervals of the line runner of the positive pole, the results shown in Table 3 are obtained.

Coordinates	Distance in, m
P (x= 0, y= 1)	$R_1 = 21.4709$
P (x= 10, y= 1)	$R_1 = 27.5862$
P (x= 20, y= 1)	$R_1 = 35.5105$
P (x= 30, y= 1)	$R_1 = 44.2831$
P (x= 40, y= 1)	$R_1 = 53.4883$
P (x= 50, y= 1)	$R_1 = 62.9364$
P (x= 60, y= 1)	$R_1 = 72.5327$

Table 3 Distance from the positive pole to the measurement point.

Performing the same procedure for the negative pole.

$$R_2 = \sqrt{(0 - 10)^2 + (1 - 20)^2}$$
$$R_2 = 21.4709 \text{ m}$$

For the rest of the intervals of the line runner of the negative pole, the results shown in Table 4 are obtained.

Coordinates	Distance in, m
P (x= 0, y= 1)	$R_2 = 21.4709$
P (x= 10, y= 1)	$R_2 = 19$
P (x= 20, y= 1)	$R_2 = 21.4709$
P (x= 30, y= 1)	$R_2 = 27.5862$
P (x= 40, y= 1)	$R_2 = 35.5105$
P (x= 50, y= 1)	$R_2 = 44.2831$
P (x= 60, y= 1)	$R_2 = 53.4883$

Table 4 Distance from pole 2 to the measurement point.

The calculation of the magnetic field components of each pole is carried out. For the positive pole, the distance R_1 to point P (x= 0, y= 1) is used, applying equations (3) and (4) as shown below.

$$B_{x_1} = \frac{\pi \cdot 4 \times 10^{-7} \cdot 3000}{2 \times 10^{-6} \cdot \pi} \cdot \left(\frac{0 - (-10)}{(21.4709)^2} \right)$$
$$B_{x_1} = 13.0151 \ \mu\text{T}$$

$$B_{y_1} = \frac{\pi \cdot 4 \times 10^{-7} \cdot 3000}{2 \times 10^{-6} \cdot \pi} \cdot \left(\frac{1 - 20}{(21.4709)^2} \right)$$
$$B_{y_1} = -24.7288 \ \mu\text{T}$$

The results obtained from the horizontal and vertical components of the positive pole are show in Table 5 and 6 respectively.

Coordinates	Component in, μT
P (x= 0, y= 1)	$B_{x_1} = 13.0151$
P (x= 10, y= 1)	$B_{x_1} = 15.7687$
P (x= 20, y= 1)	$B_{x_1} = 14.2743$
P (x= 30, y= 1)	$B_{x_1} = 12.2386$
P (x= 40, y= 1)	$B_{x_1} = 10.4858$
P (x= 50, y= 1)	$B_{x_1} = 9.0886$
P (x= 60, y= 1)	$B_{x_1} = 7.9832$

Table 5 Horizontal components of the positive pole on the line corridor

Coordinates	Component in, μT
P (x= 0, y= 1)	$B_{y_1} = -24.7288$
P (x= 10, y= 1)	$B_{y_1} = -14.9802$
P (x= 20, y= 1)	$B_{y_1} = -9.0404$
P (x= 30, y= 1)	$B_{y_1} = -5.8133$
P (x= 40, y= 1)	$B_{y_1} = -3.9846$
P (x= 50, y= 1)	$B_{y_1} = -2.8780$
P (x= 60, y= 1)	$B_{y_1} = -2.1668$

Table 6 Vertical components of the positive pole on the line corridor

ISSN: 2414-4924

For the negative pole, the distance R_2 to point P (x= 0, y= 1) is used, applying equations (3) and (4) as shown below.

$$B_{x_2} = \frac{\pi \cdot 4 \times 10^{-7} \cdot -3000}{2 \times 10^{-6} \cdot \pi} \cdot \left(\frac{0 - 10}{(21.4709)^2}\right)$$
$$B_{x_2} = 13.0151\ \mu T$$

$$B_{y_2} = \frac{\pi \cdot 4 \times 10^{-7} \cdot -3000}{2 \times 10^{-6} \cdot \pi} \cdot \left(\frac{1 - 20}{(21.4709)^2}\right)$$
$$B_{y_2} = 24.7288\ \mu T$$

The results obtained from the horizontal and vertical components of the negative pole are show in Table 7 and 8 respectively.

Coordinates	Component in, μT
P (x= 0, y= 1)	$B_{x_2} = 13.0151$
P (x= 10, y= 1)	$B_{x_2} = 0$
P (x= 20, y= 1)	$B_{x_2} = -13.0151$
P (x= 30, y= 1)	$B_{x_2} = -15.7687$
P (x= 40, y= 1)	$B_{x_2} = -14.2743$
P (x= 50, y= 1)	$B_{x_2} = -12.2386$
P (x= 60, y= 1)	$B_{x_2} = -10.4858$

Table 7 Horizontal components of the negative pole on the line corridor

Coordinates	Component in, μT
P (x= 0, y= 1)	$B_{y_2} = 24.7288$
P (x= 10, y= 1)	$B_{y_2} = 31.5789$
P (x= 20, y= 1)	$B_{y_2} = 24.7288$
P (x= 30, y= 1)	$B_{y_2} = 14.9802$
P (x= 40, y= 1)	$B_{y_2} = 9.0404$
P (x= 50, y= 1)	$B_{y_2} = 5.8133$
P (x= 60, y= 1)	$B_{y_2} = 3.9846$

Table 8 Vertical components of the negative pole on the line corridor

Sum of all contributions at a point

The sum of the contributions for the horizontal component at the measurement point P (x= 0, y= 1), is developed using equation (6).

$$B_H = 13.0151 + 13.0151 = 26.0302\ \mu T$$

Table 9 shows the results obtained from the contributions for the horizontal component on the line corridor.

Coordinates	Component in, μT
P (x= 0, y= 1)	$B_H = 26.0302$
P (x= 10, y= 1)	$B_H = 15.7687$
P (x= 20, y= 1)	$B_H = 1.2592$
P (x= 30, y= 1)	$B_H = -3.5300$
P (x= 40, y= 1)	$B_H = -3.7885$
P (x= 50, y= 1)	$B_H = -3.1500$
P (x= 60, y= 1)	$B_H = -2.5025$

Table 9 Contributions of the horizontal component

The sum of the contributions for the vertical component at the measurement point P (x = 0, y = 1), is developed using equation (7).

$$B_V = -24.7288 + 24.7288 = 0\ \mu T$$

Table 10 shows the results obtained from the contributions for the vertical component on the line corridor.

Coordinates	Component in, μT
P (x= 0, y= 1)	$B_V = 0$
P (x= 10, y= 1)	$B_V = 16.5986$
P (x= 20, y= 1)	$B_V = 15.6884$
P (x= 30, y= 1)	$B_V = 9.1669$
P (x= 40, y= 1)	$B_V = 5.0558$
P (x= 50, y= 1)	$B_V = 2.9352$
P (x= 60, y= 1)	$B_V = 1.8177$

Table 10 Vertical component contributions

Finally, the total magnitude of the magnetic field is calculated at the measurement point P (x = 0, y = 1), using equation (8).

$$B_T = \sqrt{(26.0302)^2 + (0)^2} = 26.0302\ \mu T$$

Table 11 shows the results obtained from the total magnitude of the magnetic field on the line corridor.

Coordinates	Magnetic field density in, μT
P (x= 0, y= 1)	$B_T = 26.0302$
P (x= 10, y= 1)	$B_T = 22.8947$
P (x= 20, y= 1)	$B_T = 15.7388$
P (x= 30, y= 1)	$B_T = 9.8231$
P (x= 40, y= 1)	$B_T = 6.3177$
P (x= 50, y= 1)	$B_T = 4.3056$
P (x= 60, y= 1)	$B_T = 3.0930$

Table 11 Magnetic field density over the line corridor

In Figure 7, the plotted results of the magnetic field density over the corridor of the 500 kV bipolar transmission line in HVDC are presented.

ISSN: 2414-4924

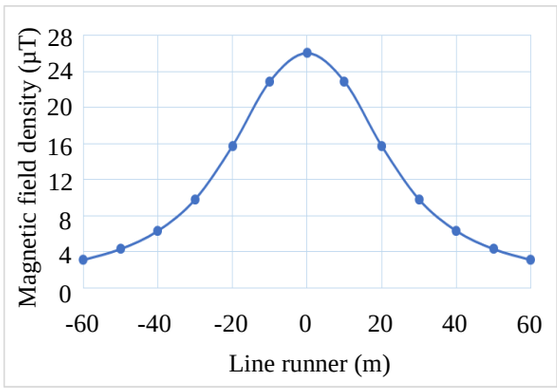

Figure 7 Magnetic field density of the 500 kV bipolar transmission line in HVDC

In Figure 7 it is observed that for the transmission line under study, the maximum magnetic field intensity is 26.0302 μT, which is lower than the maximum limit recommended by the ICNIRP.

Results

To obtain a validation of the methodology presented to calculate the density of the magnetic field, a simulation of the transmission line under study is carried out, for this the FACE software (FACE, 2019) was used, since it allows the configuration of the profiles. Transmission lines. This software is based on the complex penetration method, which uses the Carson method, which consists of the circulation of a current that returns through the earth, this method considers the earth as a superconductor, with which the return of current through the earth is modeled. Unlike the methodology presented, the FACE software uses the image conductor effect.

Table 12 and Figure 8 show the comparison of the results obtained between the methodology presented and the validation of the FACE software.

Magnetic field density	
Methodology in, μT	**FACE in, μT**
$B_{T0} = 26.0302$	$B_{T0} = 25.7698$
$B_{T10} = 22.8947$	$B_{T10} = 22.6657$
$B_{T20} = 15.7388$	$B_{T20} = 15.5814$
$B_{T30} = 9.8231$	$B_{T30} = 9.7248$
$B_{T40} = 6.3177$	$B_{T40} = 6.2545$
$B_{T50} = 4.3056$	$B_{T50} = 4.2625$
$B_{T60} = 3.0930$	$B_{T60} = 3.0620$

Table 12 Comparison of the results obtained between the methodology and the FACE software

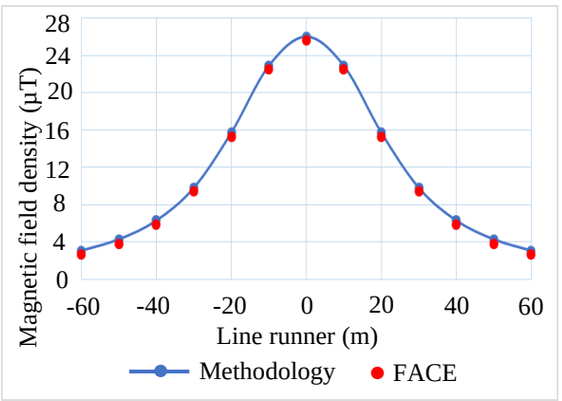

Figure 8 Comparison of the results obtained between the methodology and the FACE software

The percentage difference between the results obtained by the methodology and the FACE software is obtained with equation (9).

$$\text{dif}\,\% = \frac{M-F}{F} \cdot 100\ \% \qquad (9)$$

Where:

M = Magnetic field density obtained by the methodology proposed here, in μT.

F = Magnetic field density obtained by FACE software, in μT.

The comparison of the results obtained in interval 0 on the line corridor presented in Figure 8 and in Table 12 is made, using equation (9).

$$\text{dif}\,\% = \frac{26.0302 - 25.7698}{25.7698} \cdot 100$$

$$\text{dif}\,\% = 1.0104\%$$

Table 13 shows the percentage difference between the results obtained by the methodology and the FACE software, on the intervals of the line corridor.

Line runner intervals in, m	Percentage difference in, %
0	1.0104
10	1.0103
20	1.0101
30	1.0108
40	1.0104
50	1.0111
60	1.0124

Table 13 Percentage difference of the results obtained between the methodology and the FACE software

Analysis of the impact of the line configuration on the magnetic field density

For the analysis of the transmission line, two additional spatial configurations to the one presented in Table 1 are considered, to determine the most efficient configuration and obtain a smaller tower with a shorter line corridor.

Table 14 shows the coordinates of the poles of the second configuration of the line.

Conductor	x axis	y axis
Positive pole	-8 m	15 m
Negative pole	8 m	15 m

Table 14 Coordinates of the poles of the second configuration of the bipolar transmission line

Carrying out the methodology procedure with the second configuration of the line presented in Table 14, the results of the magnetic field density shown in Figure 9 are obtained.

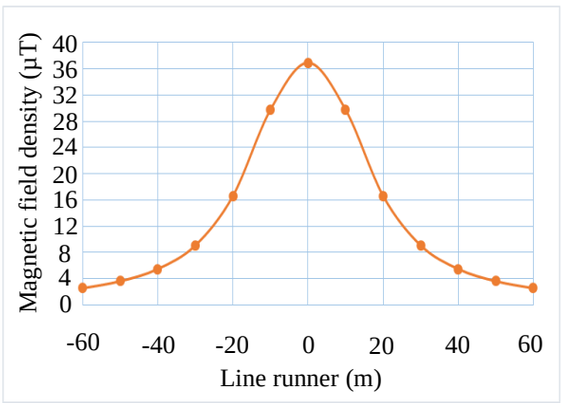

Figure 9 Magnetic field density of the second configuration of the 500 kV bipolar transmission line in HVDC

The behavior of the results obtained are typical of a transmission line, as presented in (Ahmed, Wael & Ehab, 2012).

Table 15 shows the coordinates of the poles of the third configuration of the line.

Conductor	x axis	y axis
Positive pole	-12.5 m	25 m
Negative pole	12.5 m	25 m

Table 15 Coordinates of the poles of the third configuration of the bipolar transmission line

Performing the methodological procedure with the third configuration shown in Table 15, the results of the magnetic field density shown in Figure 10 are obtained.

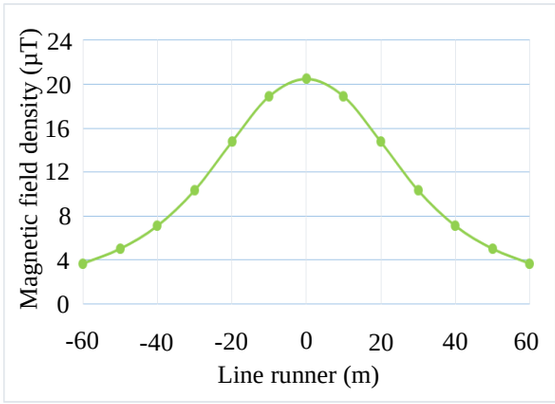

Figure 10 Magnetic field density of the third configuration of the 500 kV bipolar transmission line in HVDC

Figure 11 shows the change in the density of the magnetic field of the presented configurations, as a function of the dimensions of the tower (spacing and height) and the position of the points P.

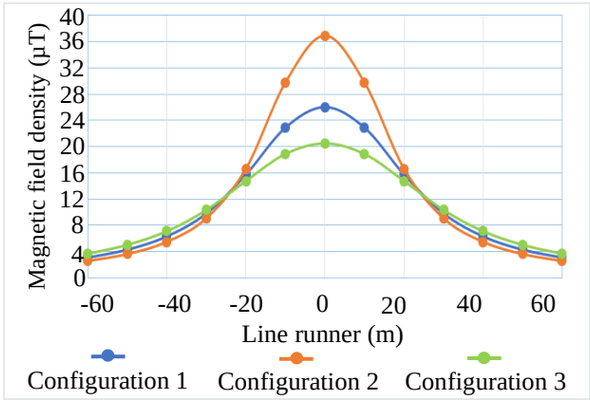

Figure 11 Magnetic field density of configurations 1, 2 and 3

The results of the magnetic field density for configurations 1, 2 and 3 are shown in Figures 7, 9 and 10, respectively, in Figure 11 the comparison of the results is observed. Configuration 3 has a lower magnetic field density, but because the transmission line has an increase in height and a greater separation of its poles, an economic increase in its installation will be generated. Due to this, it is verified that the most efficient configuration is the one presented in configuration 1 of the case study.

ISSN: 2414-4924

Conclusions

The following points are concluded from the work carried out:

- A reference methodology is presented, containing the steps necessary to perform the calculation of the magnetic field density, for the first HVDC overhead transmission lines to be built in Mexico.

- The methodology presented may be applied in bipolar and monopolar lines, admitting the different nominal voltages of the lines in HVDC, allowing to calculate the magnetic field density at a height between the poles and the ground level, over the transmission line corridor.

- The use of the presented methodology offers speed and precision, unlike commercial software like FACE generates a calculation memory of the magnetic field density in the corridor of the transmission line under study for free.

- The magnetic field density profile was validated of the 500 kV bipolar transmission line in HVDC with the FACE software, with which a difference of 1% is obtained, Because the software uses the effect of image conductor and the presented methodology does not consider it, since the effect is so small that it can be overlooked.

- It is determined that the geometry of the transmission line under study will not present magnetic field problems, as the results are less than the maximum limit recommended by the ICNIRP.

- Magnetic field density increases as the height of the poles decreases and will decrease as the distance between the poles increases.

References

Ahmed, H. Wael, M. & Ehab, M. (2012). Effect of Electromagnetic fields from Power Lines on Metallic Objects and Human Bodies.

Baharman, M. & Johnson, B. (2007). The ABCs of HVDC transmission technologies. IEEE Power and Energy Magazine.

CIGRE. (2014). CIGRE green book & overhead lines. Paris, France.

FACE. (2019). Field and corona effects, Manitoba hydro international. Canada.

Feltes, J. Gemmell, B. & Retzmann, D. (2011). From smart grid to super grid: Solutions with HVDC and FACTS for grid access of renewable energy sources. IEEE Power and Energy Society General Meeting.

Girdinio, P. Molfino, P. Nervi, M. Rossi, M. Bertani, A. & Malgarotti, S. (2015). Technical and Compatibility issues in the Design of HVDC Sea Electrodes. International Symposium on Electromagnetic Compatibility.

ICNIRP. (2009). Guidelines on limits of exposure to static magnetic fields.

IEC. (2014). IEC 62681 Electromagnetic performance of high voltage direct current (HVDC) overhead transmission lines.

IEEE. (2002). IEEE STD C95.6 Safety levels with respect to human exposure to electromagnetic fields, 0-3 kHz.

IEEE. (1994). IEEE STD Procedures for measurement of power frequency electric and magnetic fields from power lines.

Jang, Gil. Kim, Chan. Lee, Seok. Lim, Seong. & Sood, Vijay. (2009). HVDC transmission power conversion applications in power systems. John wiley & sons (Asia).

Lee, W. Pong, Philip. & Zhu, Ke. (2019). Non-contact voltage monitoring of HVDC transmission lines based on electromagnetic fields. IEEE Sensors journal, Vol. 19, No. (8).

Mooney, J. (2010). Electrical considerations for HVDC transmission lines. Power Engineers, Registered Continuing Education program RCEP.

ISSN: 2414-4924

PRODESEN. (2019). Programa de ampliación y modernización de la red nacional de transmisión y redes generales de distribución del mercado eléctrico mayorista 2019-2033.

Rofalski, K. & Schlabbach, J. (2014). Power system engineering, planning, design, and operation of power systems and equipment. John wiley & sons.

Samy, M. (2017). Computation of electromagnetic fields around HVDC transmission line tying Egypt and ksa. IEEE Nineteenth international middle aast power systems conference. Egypt.

Sarma, Maruvada, P. (2000). Corona performance of high-voltage transmission lines. Canada.

Tang, G. Luo, X. & Wei, X. (2013). Multi-terminal HVDC and DC-grid technology. Proc. Chi. Socie. Elect. Eng.

Zhou, H. Qiu, W. Sun, K. Chen, J. Deng, X. Qian, F. Wang, D. Zhao, B. Li, J. Li, S. Qiu, Y. & Yu, J. (2018). Ultra-high voltage AC/DC power transmission.

Zhu, K. Lee, W. K. & Pong, P. W. T. (2018). Fault-Line Identification of HVDC Transmission Lines by Frequency-Spectrum Correlation Based on Capacitive Coupling and Magnetic Field Sensing. IEEE Trans. Magn.

ISSN: 2414-4924

Article **ECORFAN Journal Democratic Republic of Congo**
December 2020 Vol.6 No.11 12-16

A brief description of the GPS architecture

Una descripción breve de la arquitectura del GPS

MEDINA-CASTRO, Paul†*, CARAVEO-MENA, Camilo, BARBOZA-TELLO, Norma Alicia and LOREDO-MEDINA, Raúl

Universidad Autónoma de Baja California, Faculty of Engineering Sciences and Technology, Mexico.

Instituto Tecnológico Superior de Guasave, Mexico.

ID 1st Author: *Paul, Medina-Castro* / **ORC ID:** 0000-0003-3306-1494, **CVU CONACYT ID:** 42360

ID 1st Co-author: *Camilo, Caraveo-Mena* / **ORC ID:** 0000-0001-6104-3061, **CVU CONACYT ID:** 405987

ID 2nd Co-author: *Norma Alicia, Barboza-Tello* / **ORC ID:** 0000-0002-1009-3672, **CVU CONACYT ID:** 46396

ID 3rd Co-author: *Raúl, Loredo-Medina* / **ORC ID:** 0000-0002-0785-5437, **CVU CONACYT ID:** 273827

DOI: 10.35429/EJDRC.2020.11.6.12.16 Received July 1, 2020; Accepted December 30, 2020

Abstract

The GPS is a radio-satellite system that allows to the GPS receiver to figure out its tridimensional position on the globe (latitude, longitude, and elevation), as well as allows it to determine its velocity and to make precise timing measurements. This article describes the architecture of the GPS system for the non-specialized reader. The objective is that the lector has an idea of all that happens when using some equipment or application based on this technology.

GPS, GNSS, Satellites

Resumen

El sistema GPS es un sistema de radio satelital a través del cual el usuario puede determinar su posición tridimensional (latitud, longitud y altitud), su velocidad y hacer mediciones de tiempo muy precisas. En este artículo se describe la arquitectura del sistema GPS para un lector no especializado. El objetivo es que el lector tenga una idea de todo lo que sucede cuando utiliza algún equipo o aplicación basado en esta tecnología.

GPS, GNSS, Satélites

Citation: MEDINA-CASTRO, Paul, CARAVEO-MENA, Camilo, BARBOZA-TELLO, Norma Alicia and LOREDO-MEDINA, Raúl. A brief description of the GPS architecture. Journal - Democratic Republic of Congo. 2020. 6-11:12-16.

* Correspondence to Author (Email: pmedina@uabc.edu.mx)
† Researcher contributing as first author.

Article ECORFAN Journal Democratic Republic of Congo
December 2020 Vol.6 No.11 12-16

Introduction

The Global Positioning System (GPS) is a navigation system initially developed by the US Department of Defense, and now managed by the US Air Force (U.S. Government, n.d.). The GPS idea was born at the beginning of 70's, and the whole system was completed in 1993, however it was not available for civil use until 1995. Since then, the GPS users have grown enormously around the globe, especially after the mobile's phones were provided with a GPS receiver. The GPS is a radio-satellite system that allows to the GPS receiver to figure out its tridimensional position on the globe (latitude, longitude, and elevation), as well as allows it to determine its velocity and to make precise timing measurements.

Nowadays, GPS is embedded in our daily life, in fact, our actual lifestyle would be unsustainable without GPS technology. The best-known applications of GPS are the location-based services. In this category are the vehicle or pedestrian navigation applications, which by means of the location on a map give us instructions to reach a destination. Other related applications are: 911 emergency services, children and elderly location, cab service, physical fitness applications, video games, photographs geographic labeling, personalized sales ads, etc. (Park & Kim, 2020).

In the specific case agriculture applications, GPS has allowed the development of what is known as precision agriculture (Mondal & Basu, 2009). This consists of taking samples from the ground, where each sample is labeled with its GPS location. The samples are analyzed in the laboratory to obtain information on their nitrogen and organic substance content. With this information is designed a tailored plan to treat the plot with the aim of optimizing resources such as fertilizers, irrigation, pest treatment, etc.

The GPS system is divided in three segments: the space segment, the control segment, and the user segment (U.S. Department of Homeland Security, n.d.). In the next sections of this document is explained how those segments works and how the Assisted-GPS significantly improves the accuracy and speed of the receiver measurements. After that, in the last section are reviewed additional positioning systems.

The Spatial Segment

The system requires at least 24 Medium Earth Orbit (MEO) satellites, at the date there are 7 additional backup satellites. The satellites height is around 20,200 km above the sea level, it gives them an orbital period of half a day, which guarantees the same satellites positions happening exactly at the same time each day. The satellites are carried to the space by a rocket and released on its orbit at 14,000 km/h (El-Rabbany, 2002). At this height and velocity, the satellites keep rotating on their orbit due to the equilibrium between the centrifugal force and gravity. The satellites do not require any additional source of energy for orbiting the earth, rather they require energy for the radio communication with the GPS ground stations, and for sending information to the GPS receivers. This energy is provided by batteries recharged by solar panels. The satellites distribution in their orbits guarantees that every spot-on earth is in the coverage area of at least 4 satellites.

The information is transmitted through two radio links: 1) the military band uses a radio carrier of 1,227.60 MHz, this signal is encrypted, available for the use of the US government only; 2) the civilian band uses a carrier of 1,575.42 MHz, available free of charge for every one with a GPS receiver. The signal transmitted power is just 27 W, reaching the earth surface with the extremely low power of 1.41x10-16 W, but through the use of modern techniques of coding, modulation, and signal processing the users on earth can still decode de information sent by satellites (El-Rabbany, 2002).

The information, also known as ephemerids, basically consists in the satellite position and the time of the week, both sampled at the start of transmission. The ephemerids data are 1500 bits transmitted continuously, one after another, at the very slow rate of 50 bits per second. Then the ephemerids transmission last 30 seconds. For the time measurements and as the reference for the digital circuits, the satellite uses an atomic clock, which is the most precise instrument for time measurement, it has an uncertainty of 9 ns.

ISSN: 2414-4924

The satellite radio signal is encoded by a digital sequence known as PRN (Pseudorandon Noise). Each satellite uses a unique PRN sequence that is used as the satellite identifier. The use of the PRN sequence also reduces the interference between the satellite signals and other communication systems, as well it eases and improves the synchronization between the satellite and the GPS receiver.

The Control Segment

The control segment consists of a terrestrial network that monitors the transmission of the ephemerids, analyzes the status of each satellite, and sends them synchronization and control data. A different radio link is used for the communication between the ground stations and the satellites than the one used for the transmission of the ephemeris. The ground network has a master station located in the state of Colorado, a backup master station in California, 11 command and control antennas, and 16 monitoring sites located around the globe (U.S. Government, n.d.).

The satellites are precisely tracked by ground stations whose position is precisely known; therefore, the ground network can determine the precise position of each satellite and can even send commands to the satellite to correct it, if necessary. Backup satellites can also be activated or deactivated from the terrestrial network.

It is well known that GPS satellites send weather information to ground stations, and for sure they send other kind of information for Air Force use only.

The user segment

The signal from each satellite travels towards the earth at the speed of light, and it takes about 77 ms to reach the earth's surface from the satellite. The GPS receiver on earth decodes the place and time the signal was transmitted, and then calculates the time it took for the signal to travel from the satellite to the receiver. In addition, the GPS receiver improves the accuracy of this measurement by observing the phase of the PRN code. With a standard electronic receiver, the measurement of the satellite signal delay can be measured with an accuracy of up to 10 ns.

The GPS receiver measures the signals' delay from at least four satellites. With these measurements, the receiver estimates the distance to each satellite, and since it knows the exact location of each one of them it can estimate its own position. The algorithm that runs the GPS receiver to determine its position is known as "triangulation" or "trilateration", since 3 references are sufficient to determine the position in a three-dimensional space. However, in the GPS system the fourth reference is required to reduce the uncertainty in the delays measurement, otherwise it would be required that each GPS receiver had an atomic clock, which is totally impractical and not feasible (U.S. Department of Homeland Security, n.d.).

Accuracy

As time is the measured variable, the accuracy of this measurement will determine the accuracy of the receiver position. Like already mentioned, a standard electronic receiver can measure the signal delay with an accuracy of up to 10 ns, which translates into a 3 m error in the estimation of the distance to the satellite. Thus, a standard receiver has, in theory, an error of 3 m in estimating its location.

Ideally, if it was possible that the GPS receiver to use an atomic clock, then it will be achieved an accuracy of 1 ns, which is equivalent to an error of 30 cm. This accuracy improvement is too expensive, so techniques have been developed to improve performance without highly increasing the cost of the GPS receiver. For example, military equipment receivers have access to the second GPS channel that allows them to reduce the delay measurement to 1 ns, achieving an uncertainty of 30 cm, without the use of atomic clocks.

The 3 m accuracy above mentioned is the ideal case, where the unique source of error is time uncertainty, but obviously there are more error sources. One of them is due to the propagation through the ionosphere and the troposphere, which introduce a random delay depending on the environmental conditions and the inclination. Another important source of random error is multipath propagation. It is estimated that, by accumulating the errors of all possible sources, the best accuracy can be up to 15 m (Kaplan & Hegarty, 2017).

ISSN: 2414-4924

Assisted-GPS

The time that a GPS receiver takes to synchronize with only one satellite is in between one and two seconds. Once synchronized, the satellite data decoding last at least 30 seconds, this due to the very slow transmission rate. Thus, it takes about one minute for a GPS receiver to determine its location when it starts working. After this phase, the receiver can update its position every second. In case of communication failure or if the receiver becomes out of sync, which is highly probable, another minute must elapse before the GPS receiver can update its position. This is a big problem, especially in navigation applications, for example, during the landing of an aircraft in a rainy or foggy environment.

The GPS satellites transmit exceptionally low power signals because it was designed for outdoor receivers, with line of sight to the satellites. However, due to the reduction in size and cost of the receivers, and their eminent proliferation, they are now used in places covered by vegetation, surrounded by different constructions, and inside buildings. These users observe a reduction of between 100 and 1000 times in the signal level, making it difficult to obtain information from satellites.

In Assisted-GPS, there are fixed stations which get continuous information from the satellites within their coverage area. This information is made available to nearby GPS users by using an alternative data channel of higher speed and robustness, which is usually another radio link. The GPS receivers instead of decoding the information sent by the satellites, use the information obtained from the fixed stations, so they only need to synchronize with the satellite PRN sequence to improve the estimation of their delay. The synchronization with the PRN sequence is very fast and can be achieved even with very reduced powers. Furthermore, with Assisted-GPS technique, GPS receivers can determine their location in less than a second, even if they have lost communication with the GPS satellites (Kaplan & Hegarty, 2017).

In addition, the fixed station knows its exact location, and makes a comparison it with the one obtained with their own GPS receiver, obtaining the error of the measurement. The fixed station then sends the estimated error to the mobile receivers, who use this information in order to make the correction, thus decreasing significantly the error. It is known that the Assisted-GPS techniques can achieve accuracies of less than 10 cm and connection time of less than a second. There are companies dedicated to providing the Assisted-GPS service, some of them even use geostationary satellites. In the case of cellular phones, base stations oversee provide this service, in fact, since the creation of 3G networks, Assisted-GPS was included as part of any cellular communication standard.

More Positioning Systems

GPS it is the most popular positioning system currently in operation but is not the only one. There is a Russian option called GLONASS (Global Navigation Satellite System). GLONASS initial development was parallel to that of GPS, but it was delayed by the Soviet Union collapse in 1991. GLONASS also consists of 24 satellites in orbit plus 6 backup satellites, all of them in MEO orbit at 19,100 km high (Information and Analysis Center, 2020). The Russian system is in full operation since 2011 and is included in many devices along with GPS.

China also has its own positioning system, this is called BeiDou, which is the Chinese name for the constellation we know as Ursa Major. This is a hybrid orbit satellite system, 5 GEO and 30 non-GEO (China Satellite Navigation Office, 2020). The first stage of BeiDou began operations in 2000 as a local system, serving only China and its neighbors. It is currently in operation at full capacity with worldwide coverage.

The European Union system is called Galileo. It began providing services in 2016 with half of its satellite system. It was expected that the system would be complete by the end of 2020, but this has not yet happened. Unlike the other systems, Galileo is of civil creation and management (European GNSS Agency, 2020).

ISSN: 2414-4924

This system will have a free service with features like those of GPS and GLONASS, and a paid service with much higher accuracy. The four systems are referred to under the general name of GNSS (Global Navigation Satellite System).

Conclusions

The ancient navigators used stars to locate themselves into the ocean, GPS imitates this idea, so its concept is not novel at all. Science and technology had to go a long way before mankind was able to put its own "guide stars" in the sky, and to build the "sharp eyes" that could observe them. GPS is undoubtedly one of the greatest achievements of modern engineering, which fortunately for users already has competitors. GPS was initially created for vehicle navigation and positioning, but its applications have diversified to include agriculture and entertainment, and more will surely add, as the possibilities of this technology are extensive.

References

China Satellite Navigation Office. (2020). BeiDou Navigation Satellite System. Retrieved 10 20, 2020, from http://en.beidou.gov.cn/

El-Rabbany, A. (2002). Introduction to GPS: The Global Positioning System. Artech House, Inc. Retrieved 10 2020, from https://www.gps.gov/

European GNSS Agency. (2020). What is Galileo? Retrieved 10 20, 2020, from https://www.gsc-europa.eu/galileo/system

Information and Analysis Center. (2020). Information and analysis center for posittioning, navigation and timing. Retrieved 10 20, 2020, from http://en.beidou.gov.cn

Kaplan, E., & Hegarty, C. (2017). Understanding GPS/GNSS: Principles and Applications (Third edition ed.). Artech House.

Mondal, P., & Basu, M. (2009). Adoption of precision agriculture technologies in India and in some developing countries: Scope, present status and strategies. Progress in Natural Science, 19(6), 659-666.

Park, B., & Kim, S. (2020). An effective digitized GPS signal transmission for high temporal precision IoT services. Journal of Supercomputing, 76(3), 1365–1382.

U.S. Department of Homeland Security. (n.d.). Navigation Center. Retrieved 10 20, 2020, from https://www.navcen.uscg.gov

U.S. Government. (n.d.). GPS.gov. Retrieved 10 20, 2020, from https://www.gps.gov

ISSN: 2414-4924

Article ECORFAN Journal Democratic Republic of Congo
December 2020 Vol.6 No.11 17-23

Heuristic study of a full can implementation on a network of digital controllers based on experimental data

Estudio heurístico de una implementación full can dentro de una red de controladores digitales a partir de datos experimentales

LUJÁN-RAMÍREZ, Carlos Alberto†, SANDOVAL-GÍO, Jesús*, FLORES-NOVELO, Agustín Alfonso and OJEDA-ARANA, Juan Alberto

Tecnológico Nacional De México / I.T. Mérida, Mexico.

ID 1st Author: *Carlos Alberto, Luján-Ramírez* / **ORC ID:** 0000-0002-8978-9188, **Researcher ID Thomson:** T-6838-2018, **arXiv Author ID:** clujan, **CVU CONACYT ID:** 296592

ID 1st Co-author: *Jesús, Sandoval-Gío* / **ORC ID:** 0000-0001-5847-3669, **Researcher ID Thomson:** V-1930-2018, **arXiv Author ID:** jesus.sandoval, **CVU CONACYT ID:** 297308

ID 2nd Co-author: *Agustín Alfonso, Flores-Novelo* / **ORC ID:** 0000-0002-9691-8056, **Researcher ID Thomson:** T-3024-2019, **arXiv Author ID:** afloresnovelo, **CVU CONACYT ID:** 624909

ID 3rd Co-author: *Juan Alberto, Ojeda-Arana* / **ORC ID:** 0000-0002-7239, **arXiv Author ID:** JuanOjeda, **CVU CONACYT ID:** 580342

DOI: 10.35429/EJDRC.2020.11.6.17.23 Received July 20, 2020; Accepted December 30, 2020

Abstract

Over time, the CAN (Controller Area Network) communication bus has been implemented in different technological sectors, within which, depending on the application, the bus implementation may change. On the other hand, the design and implementation of digital controls based on experimental data is a well-known topic in the automation industry where the acquisition system is of great importance. In this document, a heuristic study of the behavior of a Full CAN network is reported to implement digital controllers in two interconnected control loops. This study takes into account the access time to the bus and the amount of data sent when observing the response to disturbances. The design of two digital controllers is presented based on the parametric identification of two plants: a DC motor with an electromagnetic brake and a pneumatic levitator. Using PSoC® microcontrollers, a Full CAN network is implemented, where the digital controllers exchange data by randomly accessing the bus. A specially designed interface allows visualizing the speed and amount of data transferred under different operating conditions of the control loops. At the document end, the experimental data obtained are discussed.

Full CAN, Digital Control, PSoC

Resumen

A lo largo del tiempo, el bus de comunicaciones CAN (Controller Area Network), ha sido implementado en diferentes sectores tecnológicos, dentro de las cuales, dependiendo de la aplicación, la implementación del bus puede cambiar. Por otra parte, el diseño e implementación de controles digitales a partir de datos experimentales es un tema muy conocido en la industria de la automatización en donde el sistema de adquisición tiene una gran importancia. En este documento, se reporta un estudio heurístico del comportamiento de una red Full CAN para implementar controladoreses digitales en dos lazos de control interconectados. Dicho estudio toma en cuenta el tiempo de acceso al bus y la cantidad de datos enviados al observar la respuesta ante perturbaciones. Se presenta el diseño de sendos controladores digitales a partir de la identificación paramétrica de dos plantas: un motor de CC con freno electromagnético y un levitador neumático. Usando microcontroladoes PSoC® se implementa una red Full CAN, donde los controladores digitales intercambian datos accediendo al bus aleatoriamente. Una interfaz especialmente diseñada permite visualizar la rapidez y cantidad de datos transferida bajo distintas condiciones de operación de los lazos de control. Finalmente se discuten los datos experimentales obtenidos.

Full-CAN, Control Digital, PSoC

Citation: LUJÁN-RAMÍREZ, Carlos Alberto, SANDOVAL-GÍO, Jesús, FLORES-NOVELO, Agustín Alfonso and OJEDA-ARANA, Juan Alberto. Heuristic study of a full can implementation on a network of digital controllers based on experimental data00. Journal - Democratic Republic of Congo. 2020. 6-11:17-23.

* Correspondence to Author (Email: jesus.sg@merida.tecnm.mx)
† Researcher contributing as first author.

Introduction

The CAN communications bus was created for the interconnection of several devices without the need for dense cabling, to have a robust and economical communication with high immunity to noise. Although originally this protocol was developed for automotive applications, today it has ventured into various areas of engineering. Since the appearance of the CAN communication protocol at the end of the 80s, the bus has evolved thanks to technological advances, which allowed the inclusion of this communication bus in various areas, such as industrial, home automation, biomedical, the oil company, among others (Lawrenz, 1997). In applications destined to process control, the CAN bus has gained a lot of strength in the industrial sector, due to its low implementation costs and its reliability in high interference environments, communicating different common devices in the implementation within industrial processes (Guo, 2011) (Bailey, 2015).

The CAN communication bus is based on the OSI reference model (Open Systems Interconnection Model) where it makes use of three layers of the reference model: in the physical layer, there is a transceiver where the H and L lines are connected. of the communications bus (Bailey, 2015); Said transceiver must have the necessary electrical characteristics in accordance with the standard used (ISO11898, ISO11519, ISO11992, SAEJ2411, among others.). In the data link layer is the CAN module embedded in the controller; This module will be in charge of the logical link control and the link control to the medium. Lastly, the application layer. In this layer are the resources available by the controller for the manipulation of actuators, sensors or some interface for the final application (Bailey, 2015).

The CAN communication bus can be classified according to certain characteristics, one of them is the configuration of the buffer that receives the data of the frame, also called a mailbox (Mailbox). This configuration can have the following implementations: Basic CAN, Full CAN, FIFO, Enhaced Full CAN (Lawrenz, 1997). The most typical implementation on the bus, especially in SCDs (Distributed Control Systems), is Basic CAN (Guo, 2011) (YunxiaJiang, 2011).

Knowing the performance of the bus when processing control signals is of great importance since inherent delays and loss of information degrade the operation of the control loop. Few tools currently exist to study these phenomena in industrial applications. In this work, a heuristic study of the performance of a Full CAN (FCAN) implementation within a digital control loop, shared by two systems, is made. It describes the design of the controllers, the implementation of the bus. At the end of the document the results obtained when the control loops are subjected to disturbances are discussed.

Method

FCAN implementation in two interconnected digital control systems

For the development of this work, a CAN communications bus is implemented, where each bus node will perform a different task: one will process the digital control algorithms of each proposed system. Two systems will be studied: System 1 (S1), the control of a motor before disturbances and System 2 (S2) the control of a pneumatic levator. The implementation of the nodes and the interface of the sensors, actuators and transceivers was carried out in the CY8CKIT-059® kit, based on the CY8C5888LTI-LP097® microcontroller, from CYPRESS®.

Description of the FCAN bus implemented

The 4-node FCAN network is proposed. Each node will perform the following tasks:

Node 1. Will send and receive data from S1 to the bus. It will be used to activate sensors and relays of the assigned system. This node will be of high priority.

Node 2. Will send and receive data to the bus from S2. This node will manage the sensors and actuators of S2.

Node 3. In this node the processing of the digital controls for the S1 and S2 systems will be performed.

Node 4: This node will receive and send data from the bus to the interface through USB-HID communication.

ISSN: 2414-4924

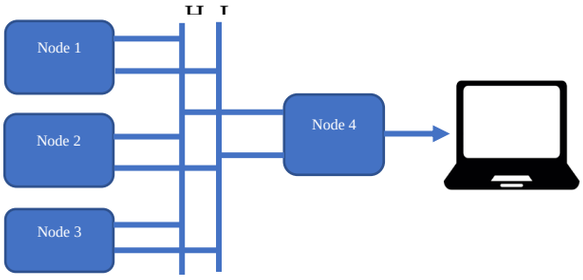

Figure 1 Structure of the network to study
Source: Self made

Systems modeling

The transfer function of each system will be found by parametric identification. The information sent or received will be continuous, which will generate a congestion of information on the bus.

The parameters for designing the controls for each system are then established.

System 1. Disturbed DC motor.

The appropriate control was designed so that at a certain disturbance (mechanical braking) of the system, it maintains its speed. S1 is made up of a 24 VDC direct current motor which, from a magnetic clutch, will induce its partial braking. The parameters to satisfy in the control will be that the system responds in no more than 1.5 seconds with less than 5% overdraft and a steady state error of 1%.

System 2. Pneumatic levator.

The S2 system is formed by a pneumatic levator. This "levitates" a disk inside a transparent tube until it reaches a desired level. The control objective is to design a controller so that the disc maintains the set position when there is a disturbance such as variation in the area of the upper air outlet window. The control that was designed complies with the following: response time of two seconds with a steady-state error less than 2%, and the overdraft must be less than 5%.

Control layout for S1.

As a first step, the transfer function of the system to be designed is obtained, by means of parametric identification.

As mentioned (Novelo, 2014) there is an extensive study of control systems, where the behavior of systems when they are excited by a specific signal is already known (Yunxia Jiang, 2011). The choice of the appropriate sensors for the acquisition of data from the system to be identified is of great importance, since a bad reading can generate an error in the determination of the transfer function. In this case, a step signal was applied to the input, setting the motor speed at 25 RPS (Revolutions Per Second) when it is being braked (disturbance). Subsequently, the brake is released and a graph of the behavior of the motor is constructed.

With the information obtained from the graph of the reaction curve, the transfer function is found. According to (Novelo, 2014), the behavior of the system corresponds to a first-order overdamped system without delay. Applying the techniques exposed by (Novelo, 2014) the transfer function of the system is:

$$G_S = \frac{1}{(.4S+1)(.4S+1)} \quad (1)$$

Graphic 1 Behavior of the engine before disturbance
Source: Self-made

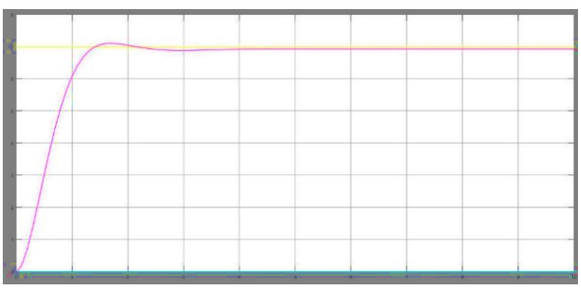

Graphic 2 Behavior of the designed control
Source: Self-made

With the transfer function of Eq. 1, proceed to design the control for the system. Following the techniques established in (M. García Juárez, 2015) (Novelo, 2014), a P-I control results.

$$\frac{s+1.7}{s+0.017} \quad (2)$$

Next, the characterization of the control in Matlab is presented.

$$\frac{s+1.7}{s+0.017} \quad (3)$$

The control design was carried out in the continuous medium, so it is necessary to convert it to the discrete medium in order to implement it in a microcontroller. To convert from the continuous medium to the discrete medium, the Tustin discretization method (Novelo, 2014) is used with the sampling time of 1 second. Subsequently, it is checked whether the discretization was correct by graphically comparing the behavior of the control in continuous medium against the discrete equivalent using simulation software such as Matlab.

Transfer function:

$$\frac{.0265z+.02243}{z^2-1.558z+.6065} \quad (4)$$

P-I control:

According to the techniques used for digital control (Novelo, 2014) (M. García Juárez, 2015), the difference equation of the designed control is obtained.

$$G_s(z) = \frac{U_z}{E_z} = \frac{z-0.8301}{z-0.9983} \quad (5)$$

$$U_{(k)} = 0.9983\,U(k-1) + E(k) - 0.8301\,E(k-1) \quad (6)$$

Obtaining the transfer function of the control 2. For the calculation of the digital control, it is necessary to know the transfer function of the pneumatic levitator. According to (Novelo, 2014) a reference is set so that a disturbance is subsequently added to the system, the disturbance is represented in Graphic 3.

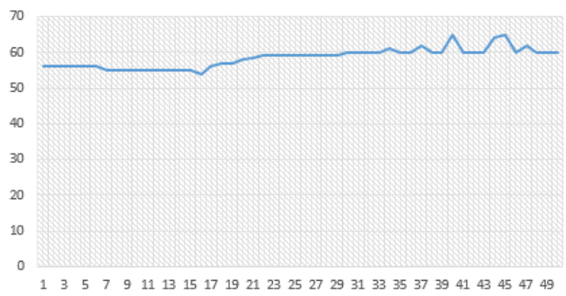

Graphic 3 System behavior S1
Source: Self-made

Using the techniques proposed in (Novelo, 2014), the resulting transfer function is:

$$G_S = \frac{1.015}{(.8S+1)(.45S+1)} \quad (7)$$

Therefore, it is necessary to design a control whose response is at least 2 seconds with a steady-state error of 2%. Using the techniques for the design of controllers in the continuous medium (Novelo, 2014) the following control is obtained:

$$\frac{s+1.2}{s+0.025} \quad (8)$$

Subsequently, the control obtained is discretized to obtain the difference equation. This equation will be the one that will be programmed into the microcontroller.

$$\frac{z-0.8801}{z-0.9975} \quad (9)$$

Experimental results

Next, the behavior of the controls in the different systems will be presented, and a comparison will be made of the number of data sent successfully on the bus with FCAN implementation of the nodes related to the control of each system. The communication bus can be classified according to the Mailbox implementation or by the type of frame and even by the type of hardware embedded in the chip. This work focuses on the Mailbox implementation, especially the Full-CAN implementation. The microcontroller used to implement the interface of the sensors, actuators and transceivers was the CY8C5888LTI-LP097® in the CY8CKIT-059® kit from the CYPRESS® company. For the visualization of the systems, an interface was developed in Visual C # ® with the possibility of saving the information in an Excel® spreadsheet.

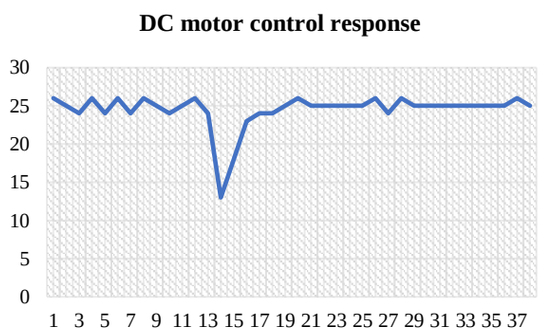

Graphic 4 Response to system disturbance S1
Source: Self-made

The PSoc Creator® facilitates the configuration of CAN modules, since it has a wizard, which reduces the amount of code to write. That said, the FCAN implementation and the assignment of the identifiers for each node was carried out successfully. One of the advantages of choosing the Full-CAN implementation in the PSoC is saving time and code, since when selecting the Mailbox as Full, values are automatically established that will make it work. The identifier, in this case, is set by the user. In a Basic-CAN implementation, the interrupts and identifiers would have to be configured via code in the PSoC Creator®.

For the configuration of the transfer speed in CAN communication at 1Mbps, it is important to have an external clock with an error less than or equal to .2%; if not, there is a risk that several messages cannot be transmitted.

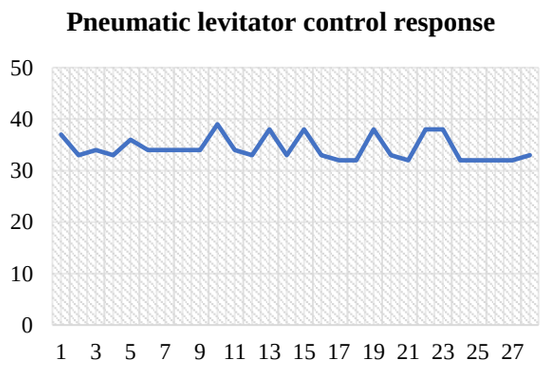

Graphic 5 Response to system disturbance S2
Source:Self-made

System control 1.

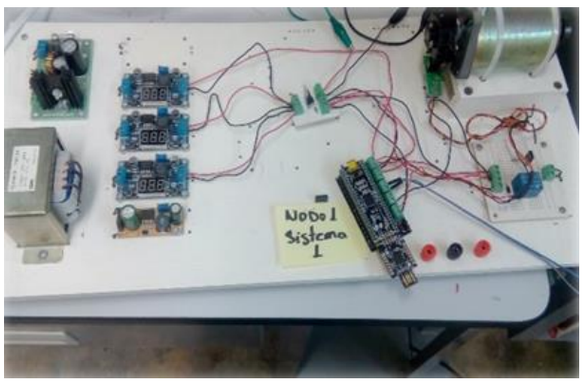

Figure 2 Control hardware 1
Source: Own elaboration

Figure 2 shows the hardware used for the implementation of the proposed system, the behavior of which is represented in Graphic 4.

The procedure followed was as follows: previously a set-point of 25 RPS is set with the brake deactivated. Subsequently, braking is activated (action represented in second 13), observing in Graphic 4 that the motor it recovers its speed in approximately 2 seconds.

System control 2.

The hardware and structure of system two can be seen in Figure 3. The testing procedure was as follows, the disk was fixed at a stable height of 36 cm, after applying a disturbance the result is shown in Graphic 5. Given the above, the system has a variation of 2 cm from the reference point.

Monitoring of data transfer on the FCAN bus

The interface created has the possibility of graphing in each second the amount of data transmitted in a specific node. This is in order to know if there is any loss of information when several nodes try to transmit at the same time. Next, in Graphic 6, the behavior of S1 is presented when only node 1 and 3 are transmitting data. As mentioned previously, node 1 oversees receiving the data from the sensors to later send it to the processing node. After being processed, the data is returned to node 1 to execute a control action on the actuator.

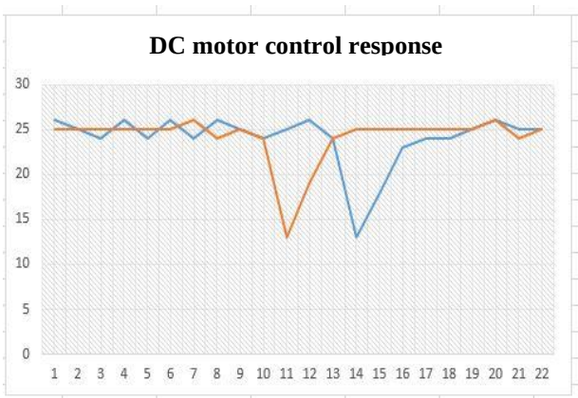

Graphic 6 S1 system control stability
Source: Self-made

The behavior of the motor in both signals is the same since it only presents a variation of 1 revolution per second. Therefore, the system is not being affected if all the elements of the CAN network request the bus to communicate with each other.

Graphic 7 shows the comparison of the control applied to system 2 when all nodes transmit versus when only nodes 2 and 3 work. The way in which the nodes communicate is as follows: node 2 is in charge of receiving information from the infrared sensor, which later, node 2 sends the data to node 3 (which applies the designed control), after the node 3 processes the information, the node returns information to node 2, this information will be used to control the actuator (motor). In the comparison of the signals of the Graphic, it is observed that in the signal where all the nodes are working (blue signal) there is greater instability.

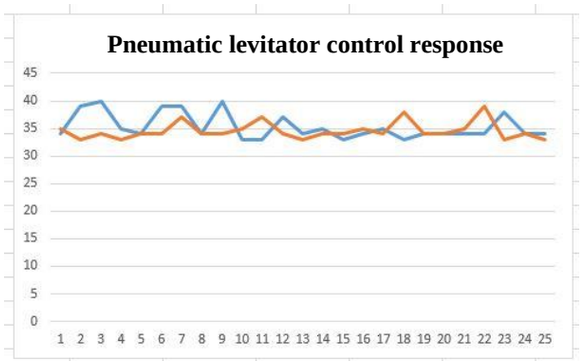

Graphic 7 S2 system control stability
Source: Self-made.

Graphic 8 presents a comparison of the data successfully transmitted by node 2 in the same cases as the previous Graphic. The blue line represents the data sent when only system 2 is working on the bus.

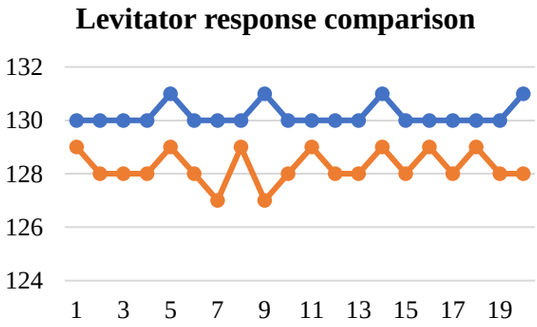

Graphic 8 Data sent on node 2
Source: Self-made

The orange signal represents the data sent when all the nodes are working. It is observed that the orange signal obtained less data sent to the processing node, it is also observed that it presents greater instability when sending data. The difference in sent / received data between the two signals is ± 4 messages.

Processing node monitoring

Graphic 9 shows the data successfully transmitted from node 3 of the CAN network. This node is in charge of processing the digital control for each system, therefore, it receives and sends information to nodes 1, 2 and 4. Graphic 9 shows two signals, one in blue and the other in orange. The first corresponds to the data sent from node 3, when only the levator system is working. The second corresponds to the data sent from node 3, when the two systems are operating. Obviously, a decrease in data sent to the nodes that will activate the corresponding actuators of each system is observed. The difference of data sent from both signals is ± 16.

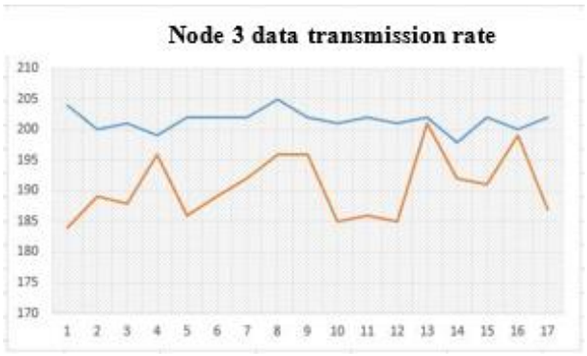

Graphic 9 Data sent from the processing node
Source: Self-made

Node	ID Previous	ID new
Node 1	0x001	0x002
Node 2	0x002	0x001
Node 3	**0x004**	**0x004**

Table 1 Full CAN identifiers
Source: Self-made

Monitoring of bus access in two nodes

Next, a comparison of the data sent is presented by changing the identifier in the FullCAN bus, where, according to (Lawrenz, 1997), the identifier 0x001 is the one with the highest priority. Graph 10 shows the comparison of the data sent by node 2. Said graph shows 2 signals. The first (blue signal) corresponds when the levator system is in operation; the second (orange signal) shows the data sent by node 2 when all the proposed systems are in operation. Comparing Graphic 9 with the current one, it is verified that there is less loss of transmitted messages when all nodes are in operation.

ISSN: 2414-4924

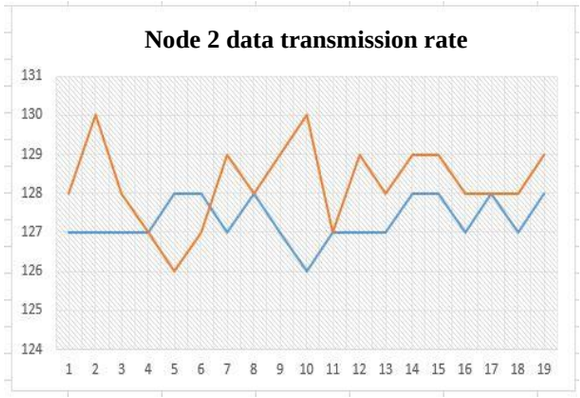

Graphic 10 Data sent on system 2 by changing the priority of nodes
Source: Self-made

Discussion

When observing the behavior of the designed controls and the availability of the nodes when communicating with each other, it was observed that, in certain nodes, the amount of data sent changes. In the levitator system, it was observed that, when all the nodes are in use, the number of messages sent decreases, said decrease, does not greatly affect the control. In contrast, Figure 10 presents the same system with modified identifiers (Table 1). The explanation for the difference in data sent from node 2 is that at the moment when two nodes want access to the bus to send data, the node with the smallest identifier wins access (Bailey, 2015) (Lawrenz, 1997) . The above mentioned is confirmed by the signals presented in Graphic 9, which correspond to node 3 whose identifier is 0x004. This graphic shows that node 4 is the one that loses the most data when all nodes are up and running. Therefore, if you want to implement several control systems in a network with Full-CAN implementation, it is recommended to assign the smallest identifiers to the nodes that need to send information more quickly.

Conclusions

Digital controllers were designed for two systems, one for controlling a DC motor and the other for a pneumatic levator. The effectiveness of the controllers designed by simulation and an experimental implementation of the same was verified. The design of the controllers was based on a parametric identification in two experiments to obtain the reaction curve of each system.

A Full CAN network was implemented where the digital controllers were embedded in a bus node. The microcontroller used to implement the interface of the sensors, actuators and transceivers was CY8C5888LTI-LP097 in the CY8CKIT-059 kit from CYPRESS. A study was carried out on the transfer of data through the bus when the nodes request access and its repercussion on the performance of the control loop.

References

Bailey, A. (2015). CAN BUS. Washington: Washington State University.

Guo, L. C. (2011). Design of the Distributed Control System Based on CAN Bus. En Computer and Information Science (págs. 83-89). Xi'an: Canadian Center of Science and Education.

Lawrenz, W. (1997). CAN system engineering from theory to practical applications. New York: Springer.

Lepkowski, J. (2004). EMI/ESD Protection. Arizona: On semiconductor.

Luo, C. L. (2013). A Co-Simulation-and-Test Method for CAN Bus System. Journal of Communications Vol. 8, 681-689.

M. Garcia Juarez, J. F. (2015). Estudio de estrategias de control PI disparado por eventos para sistemas basados en red. Congreso Nacional de Control Automatico, 447-453.

Novelo, D. A. (2014). Obtención de la Función de Transferencia de Sistemas mediante la Identificación Paramétrica a partir de datos Experimentales. En Apuntes de control. Mérida Yucatán, México.

Yunxia Jiang, B. X. (2011). Design and Implementation of CAN-Bus Experimental System. IEEE, 655-659

ISSN: 2414-4924

Article ECORFAN Journal Democratic Republic of Congo
December 2020 Vol.6 No.11 24-28

Hydrodynamic analysis of different impellers used in the stir casting process

Analisis hidrodinámico de diferentes impulsores utilizados en el proceso de stir casting

PÉREZ-PÉREZ, Arnulfo†*, MARTÍNEZ-VÁZQUEZ, J. Merced, RODRÍGUEZ-ORTIZ, Gabriel and GARCÍA-DUARTE, Oscar Enrique

Universidad Politécnica de Juventino Rosas, Metallurgical Engineering. Hidalgo 102, Community of Valencia, Santa Cruz de Juventino Rosas, Gto. 38253.

ID 1st Author: *Arnulfo, Pérez-Pérez* / **ORC ID:** 0000-0001-6354-8899, **CVU CONACYT ID:** 176434

ID 1st Co-author: *J. Merced, Martínez-Vázquez* / **ORC ID:** 0000-0002-6230-3846, **CVU CONACYT ID:** 93450

ID 2nd Co-author: *Gabriel, Rodríguez-Ortiz* / **ORC ID:** 0000-0002-3615-1973, **CVU CONACYT ID:** 48565

ID 3rd Co-author: *Oscar Enrique, García-Duarte* / **ORC ID:** 0000-0002-4781-8438, **CVU CONACYT ID:** 290387

DOI: 10.35429/EJDRC.2020.11.6.24.28 Received July 25, 2020; Accepted December 30, 2020

Abstract

In this work, the hydrodynamic behavior of four types of impellers used in the manufacture of metal matrix composites (MMC) through the stir casting process is analyzed, in order to determine which of them is adequate to generate a uniform flow in the metal. Liquid and thereby achieve a uniform distribution of reinforcing particles. The impellers analyzed are the belt type, the vane type, the propeller type and the turbine type. As a first part, the parameters of each one of them were determined to later carry out the modeling in SolidWorks. Some properties of liquid aluminum were also determined, such as density and viscosity for a melting temperature. These characteristics were assigned in the software used. As results, the flow velocities and turbulences that occur with each impeller were obtained, being the propeller-type impeller the one that shows a more uniform distribution in terms of velocities.

Impeller, Stir Casting, metal matrix composites

Resumen

En este trabajo se analiza el comportamiento hidrodinámico de cuatro tipos de impulsores utilizados en la fabricación de compuestos de matriz metálica (MMC) mediante el proceso de stir casting, con el objetivo de determinar cuál de ellos es adecuado para generar un flujo uniforme en el metal líquido y con ello lograr una distribución uniforme de partículas de refuerzo. Los impulsores analizados son el de tipo cinta, las paletas, el de hélice y el de turbina. Como primera parte se determinaron los parámetros de cada uno de ellos para posteriormente realizar el modelado en SolidWorks. También se determinaron algunas propiedades del aluminio líquido como son la densidad y la viscosidad para una temperatura de fusión. Estas características se asignaron en el software utilizado. Como resultados, se obtuvieron los regímenes de velocidades de flujo y las turbulencias que se presentan con cada impulsor, siendo el impulsor tipo hélice el que muestra una distribución más uniforme en cuanto a velocidades.

Impulsor, Stir Casting, Compuestos de matriz metalica

Citation: PÉREZ-PÉREZ, Arnulfo, MARTÍNEZ-VÁZQUEZ, J. Merced, RODRÍGUEZ-ORTIZ, Gabriel and GARCÍA-DUARTE, Oscar Enrique. Hydrodynamic analysis of different impellers used in the stir casting process. Journal - Democratic Republic of Congo. 2020. 6-11:24-28.

† Researcher contributing as first author.

Introduction

The stir casting process is used to obtain metallic matrix compounds (MMC) and was developed in 1968 when alumina particles were added to the aluminum casting. The stages in which it develops are three: the fusion of the metal, the addition of particles and stirring.

In the agitation system used, several components are necessary for its operation, these consist of a crucible which will contain the matrix material and a mechanical mixer that consists of an impeller mounted on a shaft connected to a drive unit.

Agitators are classified into axial flow and radial flow. The first allows a flow that emerges from the impeller at approximately 45 ° presenting a recirculation, returning to the central area of the impeller, creating a flow field back and forth parallel to the axis of rotation. This type of flow occurs with a Reynolds of between 200 to 600, and it becomes radial flow when the Reynolds number decreases. The second generates radial flow for any Reynolds and provides high tangential velocity but very low drive capacity.

The types of axial, radial and tangential flow will depend on the type of impeller, the characteristics and size of the fluid, as well as the proportions of the container (crucible). The velocity of the fluid at any point in the crucible has three components, and the predominant flow will depend on the variations in motion and the velocity of each component.

The radial flow is the first component of the fluid velocity, this velocity is radial and acts perpendicular to the axis of the impeller.

Longitudinal or axial flow is the second component, and it acts in a direction parallel to the axis.

Tangential or rotational flow is the third, this component acts in a tangential direction to the circular path described by the impeller.

The impellers are classified as propeller, turbine and blade (Figure 1), which are related to the types of flow already mentioned.

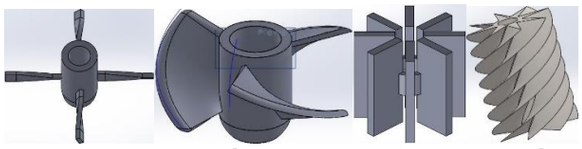

Figure 1 Impellers a) blades b) propeller, c) trubin and d) tape.
Source: Self-made

Methodology

The work was carried out by implementing numerical simulations by the finite element method by means of SolidWorks (CFD) 2018 software, where the hydrodynamic behavior of the three-dimensional flow within the stirred container (crucible) was resolved. This from the solution of the continuity equations (Eq. (1)) and Navier-Stokes (Eq. (2)) in each of the cells into which the volume under study was divided.

$$\nabla \vec{V} = 0 \tag{1}$$

$$\rho \frac{\delta \vec{V}}{\delta t} + (\vec{V} * \nabla)\vec{V} = -\nabla p + \rho \vec{g} + \mu \nabla^2 \vec{V} \tag{2}$$

The materials chosen for study were the aluminum alloy A60061 reinforced with Al_2 O_3 (alumina) particles. The mean particle size was 15.3 µm.

The parameters considered in the oven are those shown in table 1.

Element	Parameter	Value
Aluminum	melting temperatura	620°C
	casting temperature	750°C
	density	2700 kg/m3
Melting pot	material	grafito
	capacity	3.68 m3
	thickness	25.4 mm
	Diam. upper D	0.78 m
	Diam. Lower d	0.53 m
	Height H	0.90 m
Agitator	Impeller type	Paleta, hélice, turbina o cinta
	Flow type	Num. de Reynolds

Table 1 Characteristics of the oven
Source: Self-made

The volume of the crucible was determined with equation 3.

$$Vr = \pi * H * (D^2 + d^2 + D * d) \tag{3}$$

ISSN: 2414-4924

Taking into account the data in table 1, the volume of the crucible obtained is Vr= 3.69 m^3.

Since only 75% of the crucible capacity must be used at most to avoid breakdowns, the maximum mass that can be entered is $m_{max} = 2{,}500\ kg$.

For the sizing of the different impellers analyzed in this study, the relationships in Table 2 were used.

Where D_a is the diameter of the impeller, D_t is the diameter of the crucible, E is the distance from the bottom of the crucible to the impeller, H is the height of the metal, W is the width of the impeller, J is the width of the plate, L is the length of the impeller blade and f is the space between the plate and the crucible (Figure 2).

Impeller type			
Pallas	**Propeller**	**Turbine**	**Headband**
$\frac{H}{Dt}$ =1	$\frac{H}{Dt}$ =1	$\frac{H}{Dt}$ =1	$\frac{H}{Dt}$ =1
$\frac{Da}{Dt}$ =0.33	$\frac{Da}{Dt}$ =0.33	$\frac{Da}{Dt}$ =0.33	$\frac{Da}{Dt}$ =0.33
$\frac{E}{Dt}=\frac{0.17}{0.34}$	$\frac{E}{Dt}$=0.33	$\frac{E}{Dt}$=0.33	$\frac{E}{Dt}$=0.33
$\frac{W}{f}$=0.177		$\frac{W}{Da}$=0.2	
<=45º	<=25º	$\frac{g}{Da}$=0.25	<=25º
$\frac{J}{Dt}$=0.1	$\frac{J}{Dt}$=0.1	$\frac{J}{Dt}$=0.1	$\frac{J}{Dt}$=0.1
	$\frac{f}{J}$=0.02	$\frac{f}{Dt}$=0.02	$\frac{f}{J}$=0.02

Table 2 Relationships between parameters for the different drivers
Source: Self-made

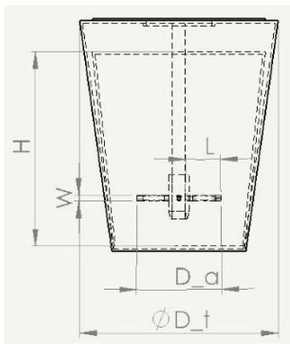

Figure 2 Parameters of a stirring system
Source: Adapted from Castillo

The density of aluminum at melting temperature (933 K to 1190 K) was determined with equation (5) proposed by Preston-Tomas

$$\rho = c_1 - c_2(T - T_{ref}) \quad (5)$$

Using data from $c_1 = 2377{,}23\frac{kg}{m^3K}$, $c_2 = 0{,}311\frac{kg}{m^3K}$, $T_{ref} = 933{,}47K$ y T =1073 K, the density was $\rho = 2333{,}84\frac{kg}{m^3}$.

Another property to take into account during the simulation was the viscosity, which was determined by equation (6).

$$Log_{10} = \frac{\mu}{\mu_o} = -a_1 + \frac{a_2}{T} \quad (6)$$

Where $\mu_o = 1mPa\,s$, $a_1 = 0{,}7324$, $a_2 = 803.49k$ and the resulting value was $\mu = 0.001035\frac{kg}{m\,s}$

In order to carry out the simulation of the study and that the parameters have a limit border, three extra pieces were developed: Two cylinders and a solid that simulated the liquid inside the crucible. One of the cylinders surrounds the impeller in all its geometry and was used to indicate the rotating section. The second cylinder is a larger one that is enveloping and containing the crucible and the entire system to be simulated. Its purpose was to contain the area where environmental forces such as pressure and gravity act.

Results

After having made the models, having entered the parameters for the simulation, and running the simulation, the resulting velocity values are shown in Figure 4 for the different impeller models analyzed.

As observed in each of the analyzes, a vortex is generated above the impeller and a vortex below it. This is most marked in the situation where the turbine impeller and the belt impeller are used.

In contrast, the impeller that generates more homogeneous flow lines is the propeller impeller.

ISSN: 2414-4924

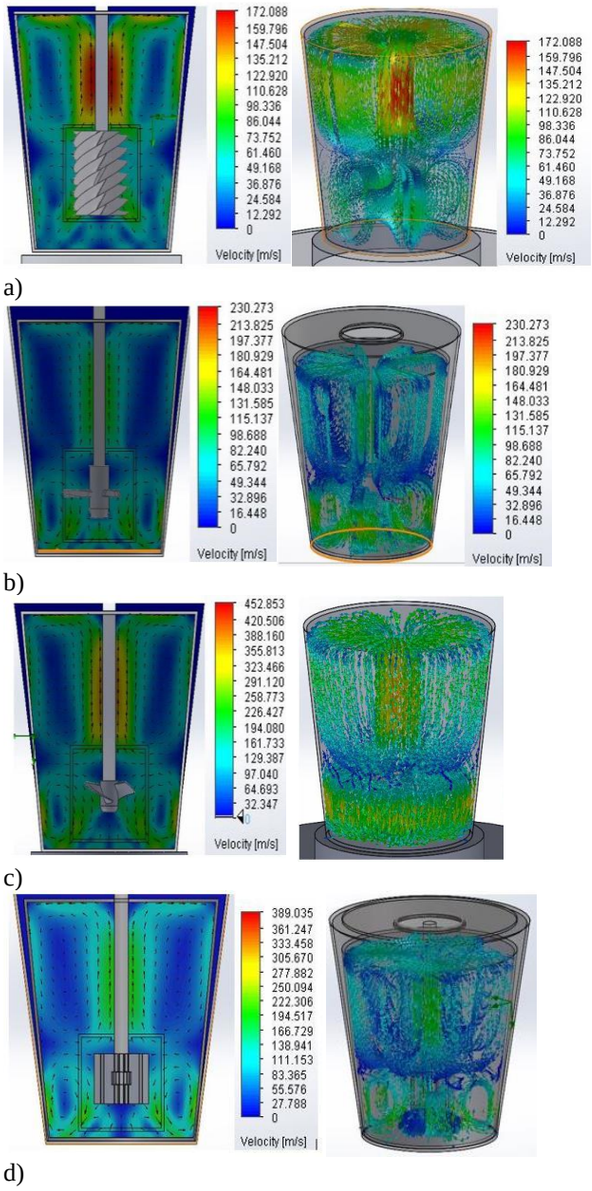

Figure 3 Speeds (m / s) obtained during the dynamic simulation with the different impeller models. a) Belt, b) Vane, c) Propeller and d) Turbine
Source: Self-made

Although the turbulence energy can be predicted in Figure 3, the values of this variable can be observed more clearly in Figure 4. The impellers that generate the highest concentrations of turbulence energy are the blades and propellers.

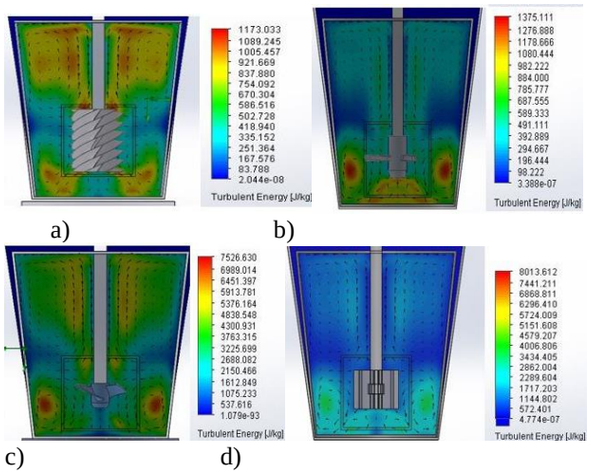

Figure 4 Turbulence energy (J / kg) obtained from the simulation when applying the various impellers. a) Belt, b) Blades, c) Propeller, d) Turbine
Source: Self-made

In the case of the turbine impeller, even when the turbulence energy values are shown constant, their values are high compared to those resulting in the other analyzes.

Conclusion

The various impeller models and the various parameters that define them, as well as the physical characteristics of the molten metals and the particles added to generate metal matrix composites, complicate the process of selecting a good stirring system for the Stir process. Casting.

However, the various finite element computer programs have come to be a great support for obtaining approximations of hydrodynamic behavior.

For this work, the SolidWorks simulation part allowed to solve the continuity equations of a stirring system with different impellers, to determine the speed and turbulence regimes inside the crucible.

The results of the simulation indicated that the propeller type impeller is the one that generates flow lines with more homogeneous speeds and that, therefore, would generate a better distribution of the particles.

ISSN: 2414-4924

References

da Costa, C. E., López, F. V., & Castelló, J. M. T. (2000). Materiales compuestos de matriz metálica. I parte. Tipos, propiedades, aplicaciones. Revista de metalurgia, 36(3), 179-192.

Hernández-Montecillo, V. M. (2019). Análisis Numérico De La Hidrodinámica En Tanques Agitados A Través De Implementar Una Turbina Rusthon. JÓVENES EN LA CIENCIA, 6.

Valencia, M., Morales, A., & Martínez, V. (2007). Compoforjado de materiales compuestos base al-si, reforzados con β-sic. Scientia et technica, 1(36).

Morales, A., Sanchez, S., Valencia, M. F., Zuluaga, C., Riaño, L. J. C., & Martínez, V. (2007). Diseño y puesta a punto de una nueva tecnologia de fundicion semisólida para composites metalicos en colombia. Scientia et technica, 1(36).

Oliveros, C. E., Alvarez, F., & Montoya, E. C. (1997). Metodología para el escalamiento de agitadores mecánicos utilizados en procesos con fluidos no-newtonianos. Revista Facultad Nacional de Agronomía Medellín, 50(1), 31-54.
Verdugo Leal, R. H. (2013). Diseño y cálculo de un agitador de fluidos.

Caneo Cartagena, E. A. (2017). Creep de compuestos de A16061/Nano A1203 fabricados por proceso de stir casting.

Peña Hechavarría, I. (2017). Construcción de un crisol de grafito para la fusión de ferroaleaciones a escala de laboratorio (Doctoral dissertation, Departamento de Mecánica).

Forn, A., Rupérez, E., Martín, E., & Picas, J. A. (2007, March). DEFORMACIÓN PLÁSTICA DEL MATERIAL COMPUESTO A6061/Al2O3p. In Anales de la Mecánica de Fractura (Vol. 1).

Taco Quispe, M. T. (2018). Estudio sobre el comportamiento mecánico de un compuesto de matriz metálica Al-SiO2 utilizando como materia prima latas de Aluminio y Cascarilla de Arroz.

Bolívar Martínez, R. D. (2013). Análisis, diseño y modelamiento por elementos finitos del eje para un agitador mecánico de la empresa Flow Control and Handling SA (Bachelor's thesis, Universidad Autónoma de Occidente).

Quispe Zuñiga, M. K. (2019). Determinación del tamaño de partícula óptimo de la sílice amorfa que actúa como reforzante en un composito de matriz metalica.

Martínez, H. V. (2007). Metalurgia semisólida de aleaciones y composites metálicos procesados por agitación mecánica. Revista latinoamericana de metalurgia y materiales, 27(1), 13-27.

Vera, S., Cortés, M., Rao, J., Fazio, P., & Bustamante, W. (2015). Evaluación de modelos de turbulencia para predecir los flujos de masa de aire interzonas a través de una abertura de escalera para la convección natural y mixta en los edificios. Revista ingeniería de construcción, 30(2), 85-97.

Gustavo, R., (2019). Modelos de turbulencia introductorio (DOI: https://www.researchgate.net/deref/http%3A%2F%2Fdx.doi.org%2F10.13140%2FRG.2.2.21060.17289)

Cercado Bueno, M. N., & Yuquilema Guamán, C. O. (2018). Diseño y construcción de un sistema de inyección y agitación para fabricación de aleaciones no ferrosas reforzadas con partículas cerámicas nanométricas (Bachelor's thesis, Espol).

Ramírez-Muñoz, J., García-Cortés, D., Colín-Luna, J. A., & Tapia-Medina, C. R. (2016). Efecto de la Evolución del Vórtice sobre los Parámetros Hidrodinámicos de un Sistema de Dispersión Mecánica de Pigmentos. Información tecnológica, 27(4), 145-154.

ISSN: 2414-4924

[Title in Times New Roman and Bold No. 14 in English and Spanish]

Surname (IN UPPERCASE), Name 1st Author†*, Surname (IN UPPERCASE), Name 1st Coauthor, Surname (IN UPPERCASE), Name 2nd Coauthor and Surname (IN UPPERCASE), Name 3rd Coauthor

Institutional Affiliation of Author including Dependency (No.10 Times New Roman and Italic)

International Identification of Science - Technology and Innovation

ID 1st Author: (ORC ID - Researcher ID Thomson, arXiv Author ID - PubMed Author ID - Open ID) and CVU 1st author: (Scholar-PNPC or SNI-CONACYT) (No.10 Times New Roman)

ID 1st Coauthor: (ORC ID - Researcher ID Thomson, arXiv Author ID - PubMed Author ID - Open ID) and CVU 1st coauthor: (Scholar or SNI) (No.10 Times New Roman)

ID 2nd Coauthor: (ORC ID - Researcher ID Thomson, arXiv Author ID - PubMed Author ID - Open ID) and CVU 2nd coauthor: (Scholar or SNI) (No.10 Times New Roman)

ID 3rd Coauthor: (ORC ID - Researcher ID Thomson, arXiv Author ID - PubMed Author ID - Open ID) and CVU 3rd coauthor: (Scholar or SNI) (No.10 Times New Roman)

(Report Submission Date: Month, Day, and Year); Accepted (Insert date of Acceptance: Use Only ECORFAN)

Abstract (In English, 150-200 words)

Objectives
Methodology
Contribution

Abstract (In Spanish, 150-200 words)

Objectives
Methodology
Contribution

Keywords (In English)

Indicate 3 keywords in Times New Roman and Bold No. 10

Keywords (In Spanish)

Indicate 3 keywords in Times New Roman and Bold No. 10

Citation: Surname (IN UPPERCASE), Name 1st Author, Surname (IN UPPERCASE), Name 1st Coauthor, Surname (IN UPPERCASE), Name 2nd Coauthor and Surname (IN UPPERCASE), Name 3rd Coauthor. Paper Title. ECORFAN Journal-Democratic Republic of Congo. Year 1-1: 1-11 [Times New Roman No.10]

* Correspondence to Author (example@example.org)
† Researcher contributing as first author.

Introduction

Text in Times New Roman No.12, single space.

General explanation of the subject and explain why it is important.

What is your added value with respect to other techniques?

Clearly focus each of its features

Clearly explain the problem to be solved and the central hypothesis.

Explanation of sections Article.

Development of headings and subheadings of the article with subsequent numbers

[Title No.12 in Times New Roman, single spaced and bold]

Products in development No.12 Times New Roman, single spaced.

Including graphs, figures and tables-Editable

In the article content any graphic, table and figure should be editable formats that can change size, type and number of letter, for the purposes of edition, these must be high quality, not pixelated and should be noticeable even reducing image scale.

[Indicating the title at the bottom with No.10 and Times New Roman Bold]

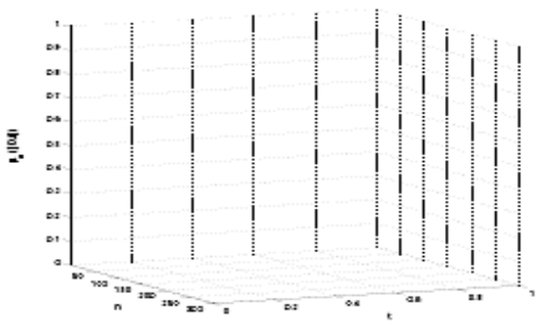

Graphic 1 Title and *Source (in italics)*

Should not be images-everything must be editable.

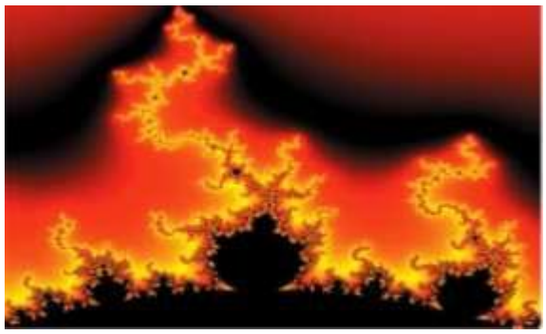

Figure 1 Title and *Source (in italics)*

Should not be images-everything must be editable.

Table 1 Title and *Source (in italics)*

Should not be images-everything must be editable.

Each article shall present separately in **3 folders**: a) Figures, b) Charts and c) Tables in .JPG format, indicating the number and sequential Bold Title.

For the use of equations, noted as follows:

$$Y_{ij} = \alpha + \sum_{=1}^{h}{}^{r} \beta_h X_{hij} + u_j + e_{ij} \quad (1)$$

Must be editable and number aligned on the right side.

Methodology

Develop give the meaning of the variables in linear writing and important is the comparison of the used criteria.

Results

The results shall be by section of the article.

Annexes

Tables and adequate sources

Thanks

Indicate if they were financed by any institution, University or company.

Conclusions

Explain clearly the results and possibilities of improvement.

ISSN 2414-4924

References

Use APA system. Should not be numbered, nor with bullets, however if necessary numbering will be because reference or mention is made somewhere in the Article.

Use Roman Alphabet, all references you have used must be in the Roman Alphabet, even if you have quoted an Article, book in any of the official languages of the United Nations (English, French, German, Chinese, Russian, Portuguese, Italian, Spanish, Arabic), you must write the reference in Roman script and not in any of the official languages.

Technical Specifications

Each article must submit your dates into a Word document (.docx):

Journal Name
Article title
Abstract
Keywords
Article sections, for example:

1. *Introduction*
2. *Description of the method*
3. *Analysis from the regression demand curve*
4. *Results*
5. *Thanks*
6. *Conclusions*
7. *References*

Author Name (s)
Email Correspondence to Author
References

Intellectual Property Requirements for editing:

-Authentic Signature in Color of Originality Format Author and Coauthors

-Authentic Signature in Color of the Acceptance Format of Author and Coauthors

ISSN 2414-4924

Reservation to Editorial Policy

ECORFAN-Democratic Republic of Congo reserves the right to make editorial changes required to adapt the Articles to the Editorial Policy of the Journal. Once the Article is accepted in its final version, the Journal will send the author the proofs for review. ECORFAN® will only accept the correction of errata and errors or omissions arising from the editing process of the Journal, reserving in full the copyrights and content dissemination. No deletions, substitutions or additions that alter the formation of the Article will be accepted.

Code of Ethics - Good Practices and Declaration of Solution to Editorial Conflicts

Declaration of Originality and unpublished character of the Article, of Authors, on the obtaining of data and interpretation of results, Acknowledgments, Conflict of interests, Assignment of rights and Distribution

The ECORFAN-Mexico, S.C Management claims to Authors of Articles that its content must be original, unpublished and of Scientific, Technological and Innovation content to be submitted for evaluation.

The Authors signing the Article must be the same that have contributed to its conception, realization and development, as well as obtaining the data, interpreting the results, drafting and reviewing it. The Corresponding Author of the proposed Article will request the form that follows.

Article title:

– The sending of an Article to ECORFAN-Democratic Republic of Congo emanates the commitment of the author not to submit it simultaneously to the consideration of other series publications for it must complement the Format of Originality for its Article, unless it is rejected by the Arbitration Committee, it may be withdrawn.

– None of the data presented in this article has been plagiarized or invented. The original data are clearly distinguished from those already published. And it is known of the test in PLAGSCAN if a level of plagiarism is detected Positive will not proceed to arbitrate.

– References are cited on which the information contained in the Article is based, as well as theories and data from other previously published Articles.

– The authors sign the Format of Authorization for their Article to be disseminated by means that ECORFAN-Mexico, S.C. In its Holding Democratic Republic of Congo considers pertinent for disclosure and diffusion of its Article its Rights of Work.

– Consent has been obtained from those who have contributed unpublished data obtained through verbal or written communication, and such communication and Authorship are adequately identified.

– The Author and Co-Authors who sign this work have participated in its planning, design and execution, as well as in the interpretation of the results. They also critically reviewed the paper, approved its final version and agreed with its publication.

– No signature responsible for the work has been omitted and the criteria of Scientific Authorization are satisfied.

– The results of this Article have been interpreted objectively. Any results contrary to the point of view of those who sign are exposed and discussed in the Article.

Copyright and Access

The publication of this Article supposes the transfer of the copyright to ECORFAN-Mexico, SC in its Holding Democratic Republic of Congo for its ECORFAN-Democratic Republic of Congo, which reserves the right to distribute on the Web the published version of the Article and the making available of the Article in This format supposes for its Authors the fulfilment of what is established in the Law of Science and Technology of the United Mexican States, regarding the obligation to allow access to the results of Scientific Research.

Article Title:

Name and Surnames of the Contact Author and the Coauthors	Signature
1.	
2.	
3.	
4.	

Principles of Ethics and Declaration of Solution to Editorial Conflicts

Editor Responsibilities

The Publisher undertakes to guarantee the confidentiality of the evaluation process, it may not disclose to the Arbitrators the identity of the Authors, nor may it reveal the identity of the Arbitrators at any time.

The Editor assumes the responsibility to properly inform the Author of the stage of the editorial process in which the text is sent, as well as the resolutions of Double-Blind Review.

The Editor should evaluate manuscripts and their intellectual content without distinction of race, gender, sexual orientation, religious beliefs, ethnicity, nationality, or the political philosophy of the Authors.

The Editor and his editing team of ECORFAN® Holdings will not disclose any information about Articles submitted to anyone other than the corresponding Author.

The Editor should make fair and impartial decisions and ensure a fair Double-Blind Review.

Responsibilities of the Editorial Board

The description of the peer review processes is made known by the Editorial Board in order that the Authors know what the evaluation criteria are and will always be willing to justify any controversy in the evaluation process. In case of Plagiarism Detection to the Article the Committee notifies the Authors for Violation to the Right of Scientific, Technological and Innovation Authorization.

Responsibilities of the Arbitration Committee

The Arbitrators undertake to notify about any unethical conduct by the Authors and to indicate all the information that may be reason to reject the publication of the Articles. In addition, they must undertake to keep confidential information related to the Articles they evaluate.

Any manuscript received for your arbitration must be treated as confidential, should not be displayed or discussed with other experts, except with the permission of the Editor.

The Arbitrators must be conducted objectively, any personal criticism of the Author is inappropriate.

The Arbitrators must express their points of view with clarity and with valid arguments that contribute to the Scientific, Technological and Innovation of the Author.

The Arbitrators should not evaluate manuscripts in which they have conflicts of interest and have been notified to the Editor before submitting the Article for Double-Blind Review.

Responsibilities of the Authors

Authors must guarantee that their articles are the product of their original work and that the data has been obtained ethically.

Authors must ensure that they have not been previously published or that they are not considered in another serial publication.

Authors must strictly follow the rules for the publication of Defined Articles by the Editorial Board.

The authors have requested that the text in all its forms be an unethical editorial behavior and is unacceptable, consequently, any manuscript that incurs in plagiarism is eliminated and not considered for publication.

Authors should cite publications that have been influential in the nature of the Article submitted to arbitration.

Information services

Indexation - Bases and Repositories

RESEARCH GATE (Germany)
GOOGLE SCHOLAR (Citation indices-Google)
REDIB (Ibero-American Network of Innovation and Scientific Knowledge- CSIC)
MENDELEY (Bibliographic References Manager)

Publishing Services

Citation and Index Identification H
Management of Originality Format and Authorization
Testing Article with PLAGSCAN
Article Evaluation
Certificate of Double-Blind Review
Article Edition
Web layout
Indexing and Repository
ArticleTranslation
Article Publication
Certificate of Article
Service Billing

Editorial Policy and Management

31 Kinshasa 6593 – Republique Démocratique du Congo. Phones: +52 1 55 6159 2296, +52 1 55 1260 0355, +52 1 55 6034 9181; Email: contact@ecorfan.org www.ecorfan.org

ECORFAN Journal-Democratic Republic of Congo

2414 4924
ISSN 2414 - 4924

www.ecorfan.org